

**Maximizing Micro-Channel Heat Transfer Efficiency with
Longitudinal Vortex Generators and Advanced Tri-Hybrid
Nano-Fluids**



By

Syed Muhammad Ahzam

(Registration No: 00000329190)

Department of Mechanical Engineering
School Of Mechanical and Manufacturing Engineering
National University of Sciences & Technology (NUST)

Islamabad, Pakistan

OCTOBER 2024

**Maximizing Micro-Channel Heat Transfer Efficiency with
Longitudinal Vortex Generators and Advanced Tri-Hybrid
Nano-Fluids**



By

Syed Muhammad Ahzam

(Registration Number: 00000329190)

A thesis submitted to the National University of Sciences and Technology, Islamabad,

in partial fulfillment of the requirements for the degree of

Master of Science in
Mechanical Engineering

Supervisor: Dr. Ammar Tariq

School Of Mechanical and Manufacturing Engineering

National University of Sciences & Technology (NUST)

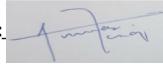
Islamabad, Pakistan

OCTOBER 2024



THESIS ACCEPTANCE CERTIFICATE

Certified that final copy of MS/MPhil thesis written by **Regn No. 00000329190 Syed muhammad Ahzam** of **School of Mechanical & Manufacturing Engineering (SMME)** has been vetted by undersigned, found complete in all respects as per NUST Statues/Regulations, is free of plagiarism, errors, and mistakes and is accepted as partial fulfillment for award of MS/MPhil degree. It is further certified that necessary amendments as pointed out by GEC members of the scholar have also been incorporated in the said thesis titled. **Maximizing Micro-Channel Heat Transfer Efficiency with Longitudinal Vortex Generators and Advanced Tri-Hybrid Nano-Fluids**


Signature: 

Name (Supervisor): Ammar Tariq

Date: 17 - Oct - 2024

Signature (HOD): 

Date: 17 - Oct - 2024

Signature (DEAN): 

Date: 17 - Oct - 2024

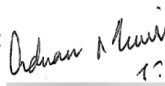
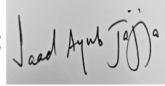




National University of Sciences & Technology (NUST)

MASTER'S THESIS WORK

We hereby recommend that the dissertation prepared under our supervision by: Syed muhammad Ahzam (00000329190)
Titled: Maximizing Micro-Channel Heat Transfer Efficiency with Longitudinal Vortex Generators and Advanced Tri-Hybrid Nano-Fluids be accepted in partial fulfillment of the requirements for the award of MS in Mechanical Engineering degree.

Examination Committee Members

- | | | |
|----|-----------------------|---|
| 1. | Name: Adnan Munir | Signature:  |
| 2. | Name: Saad Ayub Jajja | Signature:  |
| 3. | Name: Waqas Khalid | Signature:  |
| 4. | Name: Emad Ud Din | Signature:  |

Supervisor: Ammar Tariq

Signature: 

Date: 17 - Oct - 2024



Head of Department

17 - Oct - 2024

Date

COUNTERSIGNED

17 - Oct - 2024

Date



Dean/Principal

CERTIFICATE OF APPROVAL

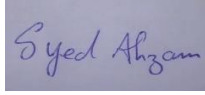
This is to certify that the research work presented in this thesis, entitled “Maximizing Micro-Channel Heat Transfer Efficiency with Longitudinal Vortex Generators and Advanced Tri-Hybrid Nano-fluids” was conducted by Mr. Syed Muhammad Ahzam under the supervision of Dr. Ammar Tariq.

No part of this thesis has been submitted anywhere else for any other degree. This thesis is submitted to the School of Mechanical and Manufacturing Engineering in partial fulfillment of the requirements for the degree of Master of Science in Field of Mechanical Engineering.

Department of SMME, National University of Sciences and Technology, Islamabad.

Student Name: Syed Muhammd Ahzam

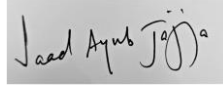
Signature:



Examination Committee:

a) External Examiner 1: Dr. Saad Ayub Jajja

Signature:



(Assistant Professor –SMME DOME)

b) External Examiner 2: Dr. Waqas Khalid

Signature:



(Assistant Professor –SMME DOME)

b) External Examiner 3: Dr Emad ud din

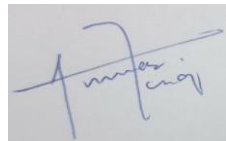
Signature:



(Professor –SMME DOME).....

Supervisor Name: Dr. Ammar Tariq

Signature:



Name of Dean/HOD: Dr. Mian Ashfaq Ali

Signature:



AUTHOR'S DECLARATION

I Syed Muhammad Ahzam hereby state that my MS thesis titled “Maximizing Micro-Channel Heat Transfer Efficiency with Longitudinal Vortex Generators and Advanced Tri-Hybrid Nano-Fluids” is my own work and has not been submitted previously by me for taking any degree from National University of Sciences and Technology, Islamabad or anywhere else in the country/ world.

At any time if my statement is found to be incorrect even after I graduate, the university has the right to withdraw my MS degree.

Name of Student: Syed Muhammad Ahzam

Date: 17-Oct-2024

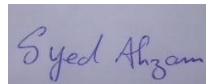
PLAGIARISM UNDERTAKING

I solemnly declare that research work presented in the thesis titled “Maximizing Micro-Channel Heat Transfer Efficiency with Longitudinal Vortex Generators and Advanced Tri-Hybrid Nano-Fluids” is solely my research work with no significant contribution from any other person. Small contribution/ help wherever taken has been duly acknowledged and that complete thesis has been written by me.

I understand the zero tolerance policy of the HEC and National University of Sciences and Technology (NUST), Islamabad towards plagiarism. Therefore, I as an author of the above titled thesis declare that no portion of my thesis has been plagiarized and any material used as reference is properly referred/cited.

I undertake that if I am found guilty of any formal plagiarism in the above titled thesis even after award of MS degree, the University reserves the rights to withdraw/revoke my MS degree and that HEC and NUST, Islamabad has the right to publish my name on the HEC/University website on which names of students are placed who submitted plagiarized thesis.

Student Signature: _____



Name: Syed Muhammad Ahzam

ACKNOWLEDGMENT

I would like to thank my thesis advisor Dr Ammar Tariq of the SMME NUST. He is the driver of my research idea, from the formulation of the problem statement to the end result of my research. He consistently allowed this paper to be my own work, but steered me in the right direction whenever he thought I needed it. His directions were succinct and encouraging.

I would also like to express my profound gratitude to Dr Adnan Munir who helped me overcome the complications of ANSYS CFD. The door to their office was always open to me whenever I ran into a trouble regarding ANSYS. I also wish to thank Dr. Emad-uddin, Dr. Saad Ayub Jajja, Dr. Waqas Khalid and Dr. Maaz Hassan for positive feedback throughout my research.

I am also thankful to my fellow lab members- Muhammad Zia ullah for his continuous support and motivation.

TABLE OF CONTENTS

ACKNOWLEDGMENT	viii
TABLE OF CONTENTS	ix
LIST OF TABLES	xi
LIST OF FIGURES	xii
LIST OF SYMBOLS, ABBREVIATIONS AND ACRONYMS	xiv
ABSTRACT	1
CHAPTER 1. INTRODUCTION	2
1.1 Micro-channels.....	2
1.2 Longitudinal Vortex Generator:	4
1.3 Nano-Fluids:.....	4
CHAPTER 2. SCOPE OF WORK	6
CHAPTER 3. LITERATURE REVIEW	7
CHAPTER 4. CFD MODEL EQUATIONS	14
4.1 Problem Statement	14
4.2 CFD Modeling.....	14
4.2.1 Single phase equations.....	15
CHAPTER 5. METHODOLOGY	17
5.1 Simulation Strategy	17
5.1.1 Geometrical Configuration	17
5.1.2 Geometry Configuration Design.....	18
5.1.3 Meshing.....	19
5.1.4 Physical model	19
5.1.5 Simulation Matrix	20

5.1.6	Material Properties.....	21
5.1.7	Boundary Condition.....	24
5.1.8	Solution methodology.....	25
5.2	Post Processing.....	26
5.2.1	Grid Independence.....	28
CHAPTER 6. RESULTS AND DISCUSSION.....		30
6.1	Data Validation.....	30
6.2	Effect of nanofluids on Nusselt Number.....	31
6.2.1	Single and Tri-Hybrid nanofluids effect.....	31
6.2.2	Effect of concentration of single & trihybrid nanofluids.....	32
6.3	Effect of Nanofluids on apparent friction factor.....	33
6.4	Effect of Nanofluids on pressure.....	34
6.4.1	Effect of comparison of 1%, 3% and 4% nanofluids on change in pressure	34
6.4.2	Effect of concentration nanofluids on change in pressure.....	34
6.5	Reynolds Number effect on base temperature.....	35
6.6	Effect of nanofluids on temperature.....	37
6.6.1	Effect on base temperature.....	37
6.6.2	Effect of concentration on Outlet temperature.....	38
6.6.3	Effect of nanofluids on Outlet temperature.....	40
6.7	Effect of nanofluids on thermal performance factor (TPF).....	42
CHAPTER 7. CONCLUSION AND FUTURE RECOMMENDATION.....		45
8.	REFERENCES.....	46

LIST OF TABLES

Table 5.1: Microchannel and LVGs model parameters.	18
Table 5.2: Simulation Matrix.	20
Table 5.3: De-Ionized Water and Properties.....	21
Table 5.4: Nanofluids Properties	23
Table 5.5 Relaxation factor	26
Table 5.6 Single Channel Mesh Characteristics.....	29

LIST OF FIGURES

Figure 1.1: Microchannel.....	4
Figure1.2 LVGs application.....	4
Figure1.3 Nanoparticles dispersion and application	5
Figure 4.1: Microchannel and LVGs geometric parameters.....	14
Figure 5.1 Microchannel and LVGs geometric parameters.....	17
Figure 5.2 Microchannel configuration	18
Figure 5.3 Meshing of microchannel and LVGs.....	19
Figure 5.4 Boundary Conditions	24
Figure 6.1: Data validation for (a) Nusselt Number (Chen. et al) and (b)friction factor (Hansel)	30
Figure 6.2: Nusselt number (Nu) comparison (a) 1% Nano-fluids (b) 3% Nano-fluids (c) 4% Nanofluids.....	31
Figure 6.3: Nusselt number (Nu) comparison of 1%,3%,4% (a)Al ₂ O ₃ (b) CuO (c) SiO ₂	32
Figure 6.4: Nusselt number (Nu) comparison of 1%,3%,4% (a) AgCuFe ₃ O ₄ (b) Al ₂ O ₃ SiO ₂ TiO ₂	33
Figure 6.5: Friction factor data of single and tri-hybrid Nanofluids	33
Figure 6.6: Pressure difference (a) 1% Nano-fluids (b) 3% Nano-fluids (c) 4% Nano-fluids	34
Figure 6.7: Pressure difference comparison of 1%, 3%, 4% (a) Al ₂ O ₃ (b) Al ₂ O ₃ SiO ₂ TiO ₂	35
Figure 6.8: Pressure contour of 4% Al ₂ O ₃ SiO ₂ TiO ₂ Re=1200 (a) Inlet (b) Outlet(c) 150° (d) 30.....	35
Figure 6.9: Temperature contours 1% Al ₂ O ₃ inlet to outlet (upward to downwards) (a) Re=1200 (b) Re=200.....	36
Figure 6.10: Velocity streamlines (a & b) and contours (c & d) around 150° and 30° LVGs	37
Figure 6.11: Temperature contours of Al ₂ O ₃ at Re=200 at (a) 1% (b) 3 % (c) 4% 38	
Figure 6.12: Outlet Temperature of 1%, 3%, 4% (a) Al ₂ O ₃ and (b) AgCuFe ₃ O 39	

Figure 6.13: Temperature contours (a&b) 150°LVGs (c&d) 30°LVGs	39
Figure 6.14: Outlet temperature of (a) 1% Nano-fluids (b) 3% Nano-fluids (c)4% Nano-fluids	40
Figure 6.15: Temperature contour at bottom of microchannel.....	41
Figure 6.16: Temperature values of fluid at bottom of microchannel.....	42
Figure 6.17: TPF of (a) 1% Nano-fluids (b) 3% Nano-fluids (c) 4% Nano-fluid	43
Figure 6.18: TPF of 1%, 3%, 4% (a) Al ₂ O ₃ SiO ₂ TiO ₂ and (b) Al ₂ O ₃	44

LIST OF SYMBOLS, ABBREVIATIONS AND ACRONYMS

L	Micro-channel model length (μm)
W	Micro-channel model width (μm)
H	Micro-channel model width (μm)
l	Vortex generator's length
w	Vortex Generator's width
h	Height of Vortex Generator
d_p	Nano Particle Dia (m)
d_f	Fluid particle Dia(m)
Nu	Nusselt Number
Re	Reynolds Number
f	Friction Factor
D_H	Hydraulic Dia (mm)
A_{ht}	Area of base of micro-channel (mm^2)
Q	Total heat rate (J/s)
\dot{m}	Flow rate (Mass) (kg/s)
\dot{V}	Flow rate (Volume) (m^3/s)
h	micro-channel height (mm)
v_{in}	Velocity at inlet (m/s)
P_{power}	Pump power (W)
ρ_f	Fluid density (kg/m^3)
C_p	Specific heat (J/kg.k)
C_f	Skin friction coefficient
μ_f	Fluid Viscosity (Pa.s)
k_f	Fluid Thermal Conductivity (W/m.k)
T_o	Outlet Tempe (K)
T_i	Inlet Temp (K)
T_m	Mean Temp (K)
T_s	Source/Base Temp (K)
ΔT	Temp Difference (K)
ΔP	Pressure Diff. (Pa)
LVG	Longitudinal Vortex Generator
P	Pressure(pa)
Pr	Prandtl number
ϕ	Nanoparticle volume fraction
μ	Dynamic Viscosity

ABSTRACT

Advancements in electronics technology have significantly improved human lives but have also introduced new challenges in managing device performance. The trend towards smaller and more portable devices has intensified the need for efficient thermal management solutions. Traditional cooling systems are often inadequate for dissipation of heat from electronic chips.

This research is based on predicting the thermal effects and hydrodynamics of single-phase micro-heat exchangers integrated with LVGs, utilizing the introduction of nanofluids via the use of CFD model equations. The geometry of the models is created in SOLIDWORKS, and numerical computations are conducted in ANSYS Fluent R21 following mesh generation in ANSYS Workbench. Nanofluids of different types and concentration are studied to find optimum nanofluid while considering pressure drop, Nusselt number and space occupied by micro-channel. Temperature boundary conditions is applied to study best concentration and type of nanofluid depending upon performance parameters including Nusselt number (Nu), drop in pressure, temperature of base and friction factors. This study conducts a simulations of the 3D laminar flow of several nanofluids in a rectangular duct featuring a longitudinal vortex generator. The finite volume approach is utilized for solving the energy, mass and momentum governing equations. The impact of nanoparticle type, Reynolds number and concentration, on the drop in pressure and coefficient of heat transfer of the nanofluids is investigated. The range of the Reynolds number was from 200 to 1200. For both the lower and LVG walls, a constant surface temperature was assumed. Eight nanofluids were considered in which Al_2O_3 , CuO, and SiO_2 , Ag, Cu, Fe_3O_4 suspended in water while two trihybrid nanofluids: Ag-Cu- Fe_3O_4 and Al_2O_3 - SiO_2 - TiO_2 suspended in ethyleneglycol. The concentrations of nanoparticles varied between 1% and 4%.

The results revealed that for trihybrid fluid Al_2O_3 - SiO_2 - TiO_2 -ethylene glycol nanofluid at 1% concentration and a RE number of 1200, the average Nusselt number was roughly 164% higher than at a RE number of 200 which participates in enhancing convective heat transfer capability of micro-channel.

Keywords: LVG, Nanofluids, Trihybrid Nanofluids, Nusselt Number, Friction Factor

CHAPTER 1. INTRODUCTION

As a result of recent developments in passive heat transfer improvement techniques and Micro-Electro-Mechanical-Systems (MEMS), there has been an increase in the demand for study into micro-scale thermal systems. These systems often require efficient heat dissipation within a limited space. Microchannels integrated with Longitudinal Vortex Generators (LVGs) represent an effective approach for improving heat transfer in these settings. To effectively design and optimize these systems, a thorough understanding of the underlying thermo-fluidic mechanisms is essential. The behavior of fluids in microchannels can differ markedly from that observed in larger-scale systems.

Transfer of energy is enabled in heat exchangers between one or multiple fluids. Conjugate transfer of heat is stated as the process of transfer of heat that takes place due to temperature differences between a fluid and an adjacent solid surface. The miniaturization of electronic devices has significantly enhanced convenience but has also introduced the critical challenge of excessive heating, which can compromise their durability. Modern electronic devices often incorporate compact circuit boards to maintain portability. Microchannels, with their small size, reduced material usage, mobility, and superior performance, have emerged as promising solutions for addressing the thermal management needs of these devices. Micro heat exchangers with LVGs and nanofluids can be employed in various applications, ranging from small consumer electronics to large-scale industrial components. These devices consist of confined spaces that constrain fluid or gas streams to flow via microchannels. The reduced dimensions of the channel result in a significant enhancement of the surface-to-volume ratio, which in turn decreases thermal resistance.

1.1 Micro-channels

In their key work from 1981 titled "High Performance Heat Sinking for VLSI," Pease et al [1] were the major contributors in the incorporation of microchannels for the purpose of heat transfer. Researchers were motivated to investigate microchannels as a potentially useful solution for heat transfer applications as a result of this collaboration. Researchers have been debating the precise meaning of the term "microchannel" for quite some time. A classification was proposed by Mehendale [2], which would have minimum

diameters varying from 1 μm to 100 μm to be specific. Kandlikar and Grande [3] suggested a slightly broader values of 10 μm to 200 μm . Obot [4] presented a more straightforward classification system that was based on the hydraulic diameter. Microchannels were defined as those that had hydraulic diameters that were smaller than one millimeter. This definition was widely adopted by many researchers, including Bayraktar and Pidugu [5], Bahrami and Jovanovich [6], and Bahrami et al. [7].

Microchannel heat sinks are an innovative alternative to the conventional finned tube heat exchangers. Such heat sinks have found widespread uses in a variety of sectors, including the refrigeration sector, the automobile sector, and the air conditioning industry. These heat sinks are often created utilizing microfabrication or precision machining processes, and they are typically fabricated from materials of good thermal conductivity, such as silicon or copper. The heat sink (figure 1.1) features a system of microchannels that facilitate the flow of a coolant fluid, whether in liquid or gas form, to effectively dissipate heat through forced convective transfer of heat. The pattern of flow in these channels consists primarily laminar, with the coefficient of heat transfer being proportionally related to both the fluid's velocity and Reynolds number. Microchannel thermal exchangers present multiple benefits compared to traditional designs. These include an elevated surface-to-volume ratio, diminished coolant needs, enhanced areas of contact between the heated part and the flowing fluid, a compact form factor, reduced material expenses, and improved performance metrics. Equation 1.1 provides good measurement method for optimizing effectiveness of microchannel heat exchangers.

$$h = Nu \left(\frac{k}{d} \right) \quad 1.1$$

A reduction in hydraulic diameter results in a rise in the coefficient of heat transfer and Nusselt number (Nu), thereby improving convective transfer of heat. The characteristics of microchannels render them particularly appropriate for use in applications including laser diode arrays, microprocessors, and high-energy laser mirrors radars.

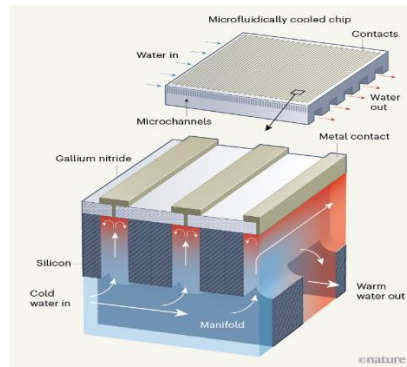


Figure 1.1: Microchannel

1.2 Longitudinal Vortex Generator:

LVGs are aerodynamic devices used to enhance flow mixing and turbulence in boundary layers. They are commonly found on aircraft wings (figure 1.2) and other aerodynamic surfaces to improve lift, reduce drag, and delay flow separation. The vortices generated interfere with the boundary layer, facilitating mixing between the primary flow and the boundary layer.

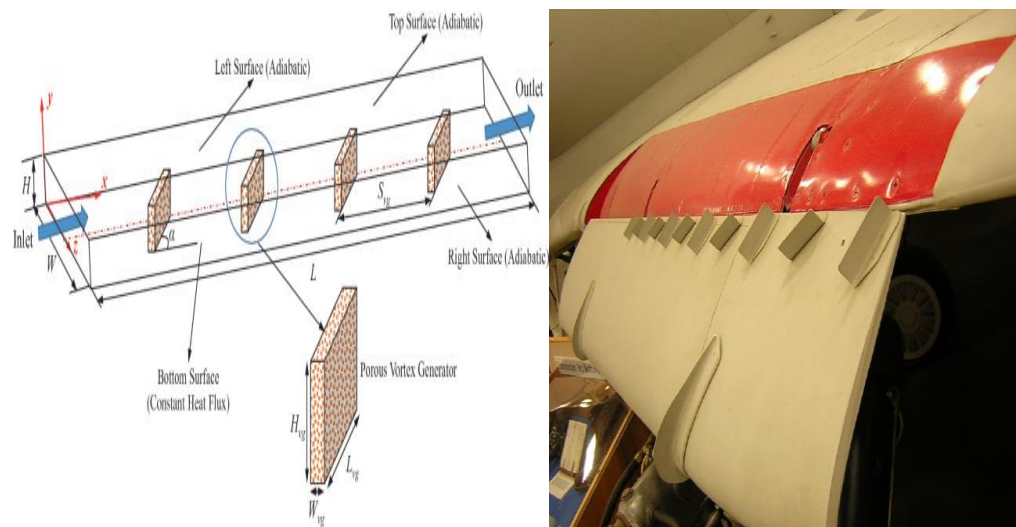


Figure1.2 LVGs application

1.3 Nano-Fluids:

Nanoparticles, defined as particles with dimensions in the nanometer range, have attracted considerable interest for their good properties to improve the heat transfer capability of base fluids. The dispersion of these nanoparticles in a base fluid result in a

suspension referred to as nanofluid. Nanofluids exhibit distinct characteristics, such as enhanced coefficients of convective heat transfer, enhanced thermal conductivity and positioning them as viable options for a range of applications, including electronics cooling, solar energy systems, and automotive engines.

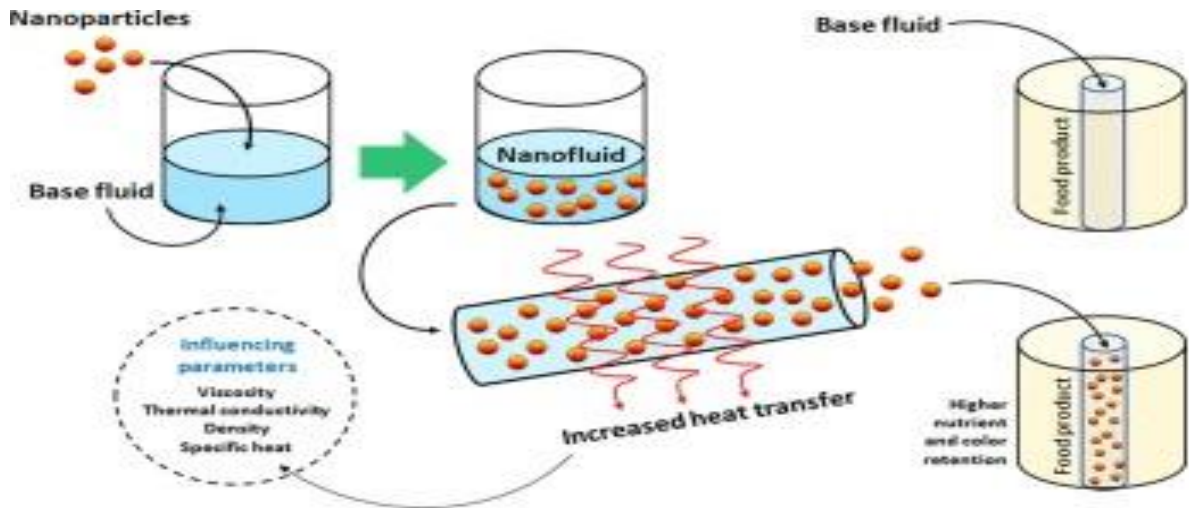


Figure1.3 Nanoparticles dispersion and application

CHAPTER 2. SCOPE OF WORK

The thermal management of microprocessors, particularly in portable and computationally intensive desktop computers, is a critical challenge that can significantly impact device performance. Water-cooled microchannels offer superior heat dissipation capabilities compared to air-cooled heat sinks. Extensive research has been conducted on straight microchannels utilizing both experimental and CFD (computational fluid dynamics) methods. However, there exists a limited body of work that investigates novel methods aimed at enhancing heat transfer by convection through geometric modifications or the incorporation of nanofluids. This study conducts a computational fluid dynamics (CFD) analysis of the flow of fluid and conjugate heat exchange in microchannels, emphasizing the role of fluid convection.

The present work studies following aspect:

1. The use of computational fluid dynamics (CFD) to simulate a microchannel, in which the heat transfer and flow behavior is investigated through the introduction of low-volume gases (LVGs) and nanofluid.
2. The verification and validation of the computational fluid dynamics (CFD) model using data from experiments sourced from existing literature.
3. Influence of Reynolds number on the friction factor and transfer of heat in micro-channels incorporating LVGs and nanofluids.
4. The impact of various nanofluids on thermal transfer performance and pressure drop characteristics.
5. Effect of varying loadings of nanoparticles (in base fluid) on the performance of micro-channels.

CHAPTER 3. LITERATURE REVIEW

This notion of tiny heat exchangers was first presented by Tuckerman [1] in 1981. Their groundbreaking research showed that liquid flow in high-aspect-ratio microchannels can markedly improve convective heat dissipation from electronic circuits. Furthermore, it was shown that rectangular microchannels demonstrated superior coefficient of heat transfer in flows of laminar relative to flow of turbulent conditions. Peng et al. [8] performed an experimental investigation on the single-phase thermal transfer properties of water passing rectangular microchannels. They investigated five different sets of the highest and lowest cross-sectional dimensions and assessed the resultant flow and heat transmission characteristics. Liquid coolants are usually chosen over gaseous coolants in microchannel heat sinks because of their higher heat transfer coefficients [9]. Harms et al. [10] experimentally established a threshold Reynolds number of 1500 for the forced convection of emerging laminar water flow in a rectangular microchannel with an estimated depth of 1000 micrometers. Their findings substantially enhance the comprehension of the change from laminar to turbulent fluid flow regimes in microchannel heat exchangers. The critical Reynolds number serves as an essential reference for engineers in the design and optimization of microchannel cooling systems, facilitating a balanced assessment of thermal transfer efficiency and pressure drop. Li et al. [11] performed numerical simulations of laminar flow transfer of heat in two non-circular microchannels with Reynolds numbers under 500. Their findings shown that in liquid flows in microchannels with a hydraulic diameter in the range of tens of micrometers, the conventional energy equations and Navier-Stokes equations under no-slip boundary conditions are applicable under the continuum hypothesis. These equations can precisely forecast the fluid dynamics and thermal transfer properties within these microchannels.

Peng et al. [12] performed experimental studies on single-phase convection that was forced in microchannels characterized by small hydraulic diameters. Their research concentrated on the impact of geometric properties on heat transfer and flow dynamics. The findings demonstrated that the aspect ratio considerably influenced laminar heat transport. Moreover, the resistance to flow in turbulent regimes was observed to be less than what classical connections anticipated.

Qu et al. [13] performed an extensive study on single-phase laminar flow within a rectangular microchannel measuring 231 by 713 micrometers. The research examined heat transfer and pressure drop characteristics, utilizing heat fluxes of 100 and 200 W/cm² at the channel's base. The numerical and experimental findings exhibited remarkable concordance, confirming the precision of the computational model. Meshan et al. [14] performed an experimental investigation on the flow and transfer of heat properties within a microchannel. Their results, derived from transfer of heat and pressure drop measurements, indicate that traditional theories of flow dynamics and entrance length effects are still relevant to microchannel flows. Lee et al. [15] performed experimental studies on the effects of water-based nanofluids with low concentrations of Al₂O₃ nanoparticles on the effectiveness of heat transfer. They noted that these nanofluids improved heat transfer coefficients in laminar flow conditions, especially at the entrance region of the microchannel. Nevertheless, the enhancing effect is less significant in completely developed flow zones. Under two-phase flow circumstances, nanoparticle clusters were detected at the channel exit, indicating localized boiling events.

Shah [16] derived an analytical expression for predicting the friction factor in rectangular microchannels, incorporating the aspect ratio and Poiseuille number relationship.

Qu et al. [17] performed an extensive computational analysis of heat transport and flow dynamics in three-dimensional rectangular microchannels. The research examined thermally and hydrodynamically emerging flow regimes, analyzing the effect of Reynolds number on the length of a developing fluid area. Moreover, the scientists illustrated that the temperature distribution in both the fluid and solid phases could be precisely represented by a linear correlation along the flow direction. Fedorov et al. [18] performed a 3-D conjugate thermal transfer investigation, determining that thermophysical properties of the materials were contingent upon temperature. Their analysis demonstrated a consistent average wall temperature distribution along the flow direction within the channel, but irregularities were noted near the inlet.

Amirah [19] performed an extensive analysis of single as well as multi-channel micro heat exchanger designs across various hydraulic diameters. Through precise numerical simulations and experimental measurements, she established that the shift from laminar to turbulent flow regimes happened at a RE of 1600. The investigation demonstrated a substantial conjugate heat transfer effect, leading to inconsistencies between the computational and experimental results.

The relevance of traditional heat and flow transfer theories to micro-scale systems has been a topic of continuous discussion. Although certain investigations have contested conventional notions [[20],[21]], others have identified negligible differences between micro- and macro-scale flow and heat transmission characteristics [[22],[23],[10]]. The inconsistencies identified throughout the scientific literature can be ascribed to scaling effects, errors from viscous heating, surface roughness, temperature-dependent characteristics, entry effects, and conjugate transfer of heat.

Axial wall conduction is a critical issue concerning scaling effects that might reduce the thermal efficiency of microchannel heat exchangers. Experimental and numerical studies have shown that enhancing the thermal conductivity of microchannel walls can increase axial wall conduction, hence diminishing thermal efficiency [[24], [25]]. Therefore, materials exhibiting poor thermal conductivity are frequently favored for microchannel heat exchangers to reduce the effects of axial wall conduction.

Numerical simulation tools have become indispensable in predicting the behavior of microchannels, offering greater flexibility in design exploration and facilitating the evaluation of potential modifications based on cost-benefit analysis. Liu and Garimella's [26] numerical investigation of microchannel heat exchangers established that the performance of rectangular microchannels with hydraulic diameters between 244 and 974 micrometers aligned with the behavior of conventional micro-channels under laminar flow conditions. Xu et al. [27] performed computational simulations to examine the flow properties of liquid in micro-channels having hydraulic diameters from 30 to 344 micrometers at Reynolds numbers between 20 and 4000. Their findings indicating the flow behavior within those microchannels conformed to the predictions of the Navier-Stokes

equations, implying that the disparities noted in previous investigations may be ascribed to inaccuracies in dimensional measurements. Hetsroni [[28],[29]] performed extensive numerical simulations of laminar flow in micro heat exchangers, integrating realistic channel geometry, energy dissipation, axial wall conduction, and temperature-dependent fluid characteristics. The numerical results exhibited strong concordance with data from experiments, confirming the precision of the computational model. Allen [30] performed experimental and numerical analyses of fluid dynamics and thermal transfer in copper micro-heat exchangers exposed to a constant temperature heat source. Although the experimental results aligned closely with CFD simulations, inconsistencies were noted when juxtaposed with theoretical expectations, especially inside the laminar flow zone.

Heat transfer enhancement strategies may be classified into active methods, which necessitate external energy, and passive methods, which do not. Passive heat transfer improvement methods include flow interruption, channel curves, fluid additives, mixing from outside plane, auxiliary flows, re-entrant obstacles, and roughness of the surface. Passive heat transfer improvement methods include flow interruption, channel curvature, fluid additives, out-of-plane mixing, secondary flows, re-entrant obstacles, and surface roughness. Furthermore, these strategies can be categorized according to their ability to improve heat transmission in the primary flow or via secondary flow mechanisms. [[31],[32],[33]]. In 1969, Johnson and Joubert initiated research on vortex generators (VGs) and their influence on thermal transfer efficiency [34]. Vortex generators can be realized in several configurations, such as ribs, winglets, wings, slanted blocks, and protrusions [35]. The variation in pressure across a vortex generator induces flow separation from its lateral edges, resulting in the formation of transverse, longitudinal, and horseshoe vortices [[36],[37],[38]]. The prevailing vortex type is contingent upon the angle of attack of the vortex generator: longitudinal vortices are predominant at low angles, whereas transverse vortices are prominent at right angles [[39],[40]]. The created vortices disrupt the flow boundary layer, disrupt the temperature field in the channel, induce auxiliary flow, and enhance the conveyance of central flow near the wall and vice versa [35]. Fiebig et al. [41] conducted experimental tests revealing that in laminar flow regimes local heat transfer can be enhanced by as much as threefold in channels using vortex generators compared to those lacking them. Wu and Tao [42] performed numerical

and experimental investigations to evaluate the influence of various attack angles of winglet on heat transfer efficiency. The average Nusselt number of the surfaces was found to increase with rising attack angles. Vortices in longitudinal direction often demonstrated enhanced heat transfer efficiency and reduced flow losses in comparison to vortices in transverse direction [[32],[39]].

Liu et al. [43] examined the application of winglet VG with differing quantities of angle of attack and pairs of VGs to improve the transfer of heat in microchannels at RE ranging from 170 to 1200. A significant enhancement in the transfer of heat was noted, but with an increased pressure drop. Furthermore, they observed a reduction in the range of critical Reynolds numbers when LVGs are integrated, in contrast to microchannels devoid of LVGs. Chen et al. [44] built upon the studies of Liu et al. by investigating various microchannel layouts with differing hydraulic diameters and heights. Lan et al. [45] performed computational simulations to analyze flow properties and transfer of heat in a rectangular microchannel featuring dimples/protrusions, with Reynolds numbers spanning from 100 to 900. Their findings suggested that the dimple/protrusion approach could improve the transfer of heat, albeit at the expense of heightened pressure drop.

One other passive methods include nanofluids which consist of different sizes and materials and concentration in any base fluid in which those can suspend. Sidik et al. [46] conducted a comprehensive review of passive heat transfer enhancement techniques for microchannel heat sinks. Their analysis revealed that the utilization of nanofluids as an alternative working fluid offers significant potential for improving thermal efficiency. Numerous studies on nanofluids and microchannel devices have confirmed the efficacy of these passive techniques in enhancing heat transfer capabilities [[47],[48]].

Pantzali et al. [49] performed an extensive investigation on the effects of nanofluids inside heat exchangers. Their findings indicated that replacing water with nanofluids markedly improved the heat transport rate. The convective heat transfer properties of nanofluids have been thoroughly examined across various nanoparticle geometries, dimensions, and compositions, as well as under diverse flow circumstances [50]. Williams et al. [51] performed experimental investigations on turbulent transfer of heat

characteristics utilizing Zirconia and Alumina nanoparticles dispersed within a tube. Their findings indicated that utilizing effective thermophysical parameters for dimensionless number calculations allows for reliable predictions of pressure drop and heat transfer characteristics of nanofluids in fully developed turbulent flow through single-phase flow models. Rea et al. [52] documented same findings for laminar flows of identical nanofluids. The literature encompasses multiple numerical simulations of convective heat transfer in various nanofluids, including CNT [[53],[54],[55]], CuO [[56],[57],[58],[59]], TiO₂ [[60],[61]], Cu [[62],[63]], and Al₂O₃ [[64],[65]], across diverse flowing geometries, such as straight tubes and curved pipes. Behzadmehret et al. [66] demonstrated that the incorporation of 1% Cu nanoparticles into the base fluid enhances the Nusselt number by over 15%, while exerting no significant influence on the skin friction coefficient. Bianco et al. [[67],[68]] indicated that the convective heat transfer coefficient for Al₂O₃-H₂O nanofluids surpasses that of the base liquid, and the boost in heat transfer escalates with increasing particle volume concentration and Reynolds number.

H.E. Ahmed et al. [69] numerically and computationally simulate the triangular LVG in a duct by incorporating various nanoparticles at concentrations ranging from 1% to 6% in base fluid. This study demonstrates an enhancement in heat transmission with the simultaneous incorporation of LVG and nanoparticles

The integration of LVGs with nanoparticles in microchannels for electronic cooling exhibits potential; nevertheless, additional study is required to fully elucidate the fundamental transfer of heat and flow dynamics. Significantly, numerical evaluations of microchannels with rectangular LVGs and diverse nanoparticle types, including hybrid and tri-hybrid configurations, have not been addressed in the literature. This thesis conducts three-dimensional simulations to examine the conjugate heat transfer characteristics and liquid flow behavior in rectangular microchannels integrated with LVGs and nanoparticles, given the promising potential of this advanced technique for enhancing heat transfer. A finite-volume approach is utilized to acquire comprehensive data on the local fluctuations of flow parameters during liquid flow via microchannels containing LVGs and nanoparticles. The impact of various nanoparticle materials, their concentrations, and Reynolds number on heat exchange and flow properties in the laminar regime is thoroughly

analyzed. This study is, to the author's knowledge, the first numerical examination of the synergistic effects of LVGs and nanoparticles in microchannels.

CHAPTER 4. CFD MODEL EQUATIONS

4.1 Problem Statement

A numerical simulation was done in 3D to examine laminar heat transfer caused by convection and nanofluid flowing in a heated rectangular channel featuring a VG. As can be visualized in Figure 4.1, the computational domain comprised of a base wall, heated LVGs, and two adiabatic side walls. The heated surfaces were set to a temperature of 323.15 K constant value. The nanofluid entered the duct with a uniform temperature, T_{in} (298K), and exited with a temperature of T_{out} . Velocities of nanofluid corresponds to 200 to 1200 Reynolds number which is in the region of laminar. The changes in convective heat transfer were evaluated using the Nusselt number as a reference, while the change in pressure was measured through the friction factor.

4.2 CFD Modeling

This research focuses on laminar, single-phase flow with steady-state of an incompressible, homogeneous nanofluid mixture with base fluid [70] within a microchannel heat exchanger model incorporating longitudinal vortex generators (LVGs). The model involves solving equations for continuity, momentum and energy while accurately capturing thermal behavior of those microchannel heat exchanger. Following figure shows the task distribution for CFD analysis

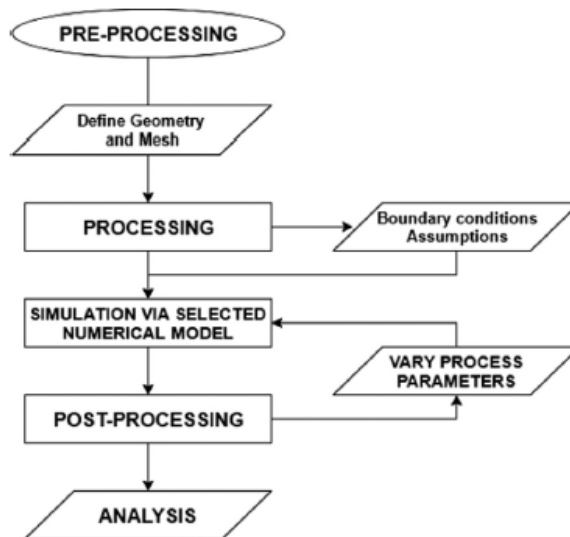


Figure 4.1: Microchannel and LVGs geometric parameters

4.2.1 Single phase equations

Solving equations of momentum and continuity have been solved to ascertain field of velocity, whereas the equation of energy is employed to compute the distribution of temperature and coefficient of wall heat transfer. Subsequent equations illustrate the momentum, mass and energy conservation:

4.2.1.1 Mass Equation (conservation)

Conservation of mass or continuity equation in its general form is written as follows along with simplified form.

$$\frac{\partial \rho}{\partial t} + \nabla \cdot (\rho \vec{v}) = S_m \quad 4.1$$

$$\frac{\partial u}{\partial x} + \frac{\partial v}{\partial y} = 0$$

In this equation t is time, v is velocity ρ is density, whereas S_m is mass added to continuous phase from user-defined sources or from second phase this general form can be used in both incompressible and compressible flows.

4.2.1.2 Momentum Equation (conservation)

Equation of momentum in an inertial frame of reference is given by

$$\frac{\partial}{\partial t} (\rho \vec{v}) + \nabla \cdot (\rho \vec{v} \vec{v}) = -\nabla p + \nabla \cdot (\bar{\tau}) + \rho \vec{g} + \vec{F} \quad 4.2$$

$$\bar{\tau} = \mu \left[(\nabla \vec{v} + \nabla \vec{v}^T) - \frac{2}{3} \nabla \cdot \vec{v} I \right] \quad 4.3$$

In the given equation, $\rho \vec{g}$ is body force due to gravity, p is static pressure, $\bar{\tau}$ is stress tensor, \vec{F} is body force from external, I is unit tensor, μ is molecular viscosity and $\nabla \vec{v}^T$ is volume dilation effect.

4.2.1.3 Energy Equation

Energy is solved by ANSYS Fluent in following form:

$$\frac{\partial}{\partial t}(\rho E) + \nabla \cdot (\vec{v}(\rho E + p)) = \nabla \cdot \left(k_{eff} \nabla T - \sum_j h_j \vec{J}_j + (\bar{\tau}_{eff} \cdot \vec{v}) \right) + S_h \quad 4.4$$

$$E = h - \frac{p}{\rho} + \frac{v^2}{2} \quad 4.5$$

In the given equation, \vec{J}_j is diffusion flux of J species, k_{eff} is effective conductivity which includes turbulent thermal conductivity when turbulent model is used. The three terms of right side in equation represents species diffusion, effective conduction and viscous dissipation whereas fourth term heat due to chemical reaction and volumetric heat sources.

CHAPTER 5. METHODOLOGY

5.1 Simulation Strategy

5.1.1 Geometrical Configuration

Three-dimensional numerical simulations were performed on a specific configuration of the microchannel. Geometry is constructed in Design Modeler with a fixed length of 20 mm. The microchannels included two sets of rectangular LVGs. Figure 5.1 depicts the geometry and relevant dimensions of the constructed microchannels. The dimensions of the microchannel are denoted as length (L), width (W), along with height (H). The height of the LVG is equivalent to the height of the microchannel, with a length denoted as l and a thickness expressed as b , as illustrated in figure 5.1. The flow has been defined within a Cartesian reference, with x , y , and z denoting the span-wise, normal, and stream-wise coordinates, respectively. The winglet pitch orientation was aligned with the y -axis, as illustrated in figure 5.2. All measurements and angles are presented in Table 1.

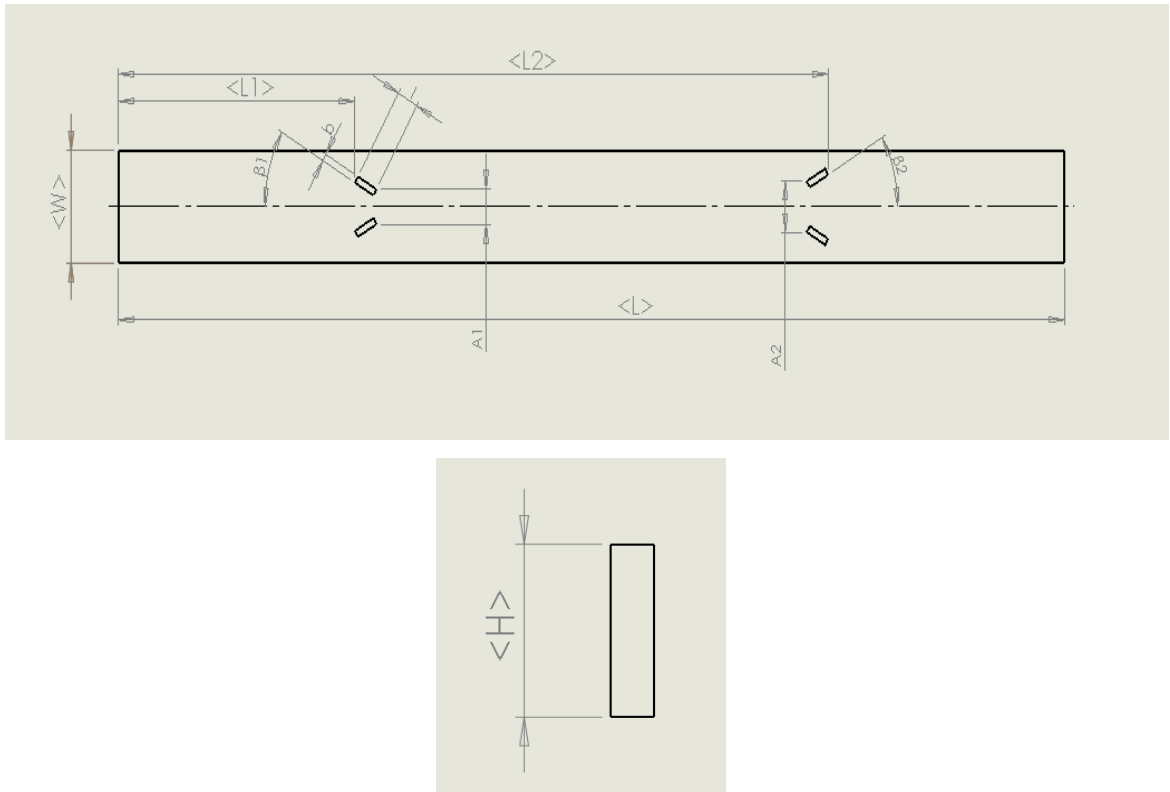


Figure 5.1 Microchannel and LVGs geometric parameters

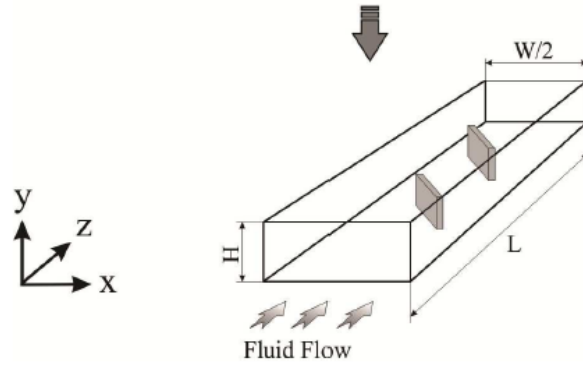


Figure 5.2 Microchannel configuration

5.1.2 Geometry Configuration Design

Rectangular Microchannel is utilized for good flow distribution of fluid according to scientific studies. Side inlet and outlet is used for fluid entrance and leaving. Balaji [71] investigated that inlet and outlet should be in a line with micro-channel for even pressure drop. Also Ebrahimi [72] in his research concluded this configuration for rectangular LVGs in rectangular microchannel provides more convective heat transfer. Additionally we have added length of 9.6mm before inlet to accommodate fully developed flow at inlet.

Table 5.1: Microchannel and LVGs model parameters.

Symbol	Dimension (μm)
L	20000+10000
W	400
H	100
L	100
B	25
H	100
L1	5000
L2	10000
a1	90
a2	40
β_1	30° (150°)
β_2	30°

The total length of the geometry is 30mm in which 10mm is accounted for hydrodynamic length fully develop flow for laminar region which is calculated from [73]:

$$L_h \approx 0.05ReD_h$$

5.1.3 Meshing

Meshing is done in ANSYS R21 build-in mesh generator module. Structured mesh is developed for single channel model shown in Fig. 5. For single model, mesh quality parameters are studied and maintained.

Maximum aspect ratio of 1.1, Minimum mesh orthogonality of 0.86734 and maximum skewness of 0.05 is achieved for microchannel having LVGs. Localized meshing around LVG is has increased for better visualization of flow.

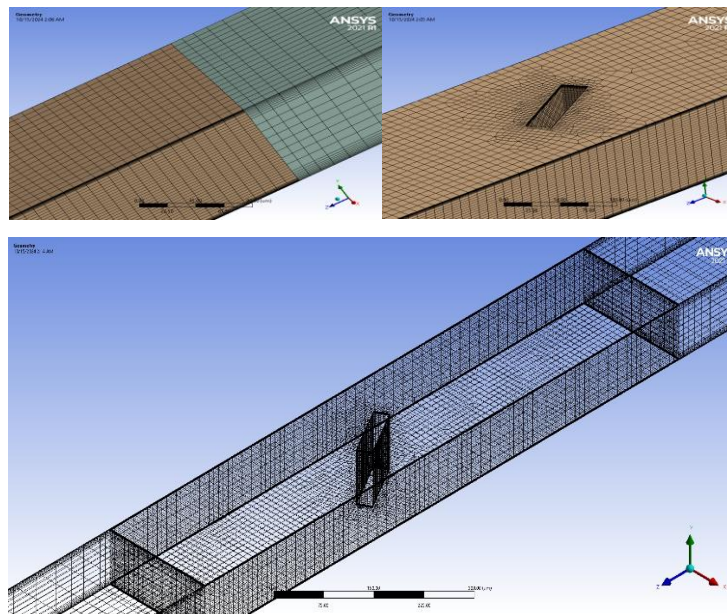


Figure 5.3 Meshing of microchannel and LVGs

5.1.4 Physical model

A viscous laminar model based on the Reynolds number, coupled with the scheme for pressure-velocity i.e. SIMPLE, was used in the numerical simulations. Second-order upwind discretization [19] was utilized for spatial terms. The convergence criterion for the

governing set of equations was set at 10^{-5} . Also conduction effect of base material where temperature boundary condition is given

5.1.5 Simulation Matrix

This study involves CFD simulation of heat transfer and fluid flow in microchannel having LVGs and nanofluids. For achieving study goal, an optimum concentration and type of nanofluid will have to be selected. A test matrix is developed as shown in Table 5.2, in which numerical simulation on different models with geometry and varying type and concentration of nanofluid against several Reynolds number is performed.

Table 5.2: Simulation Matrix.

Sr. no	Name of Nano fluid	Concentration of each nanoparticle	Reynolds Number	Cases
1	Al ₂ O ₃ -Water	1%	200-1200	6
2	Al ₂ O ₃ -Water	3%	200-1200	6
3	Al ₂ O ₃ -Water	4%	200-1200	6
4	CuO-Water	1%	200-1200	6
5	CuO-Water	3%	200-1200	6
6	CuO-Water	4%	200-1200	6
7	Ag-Water	1%	200-1200	6
8	Ag-Water	3%	200-1200	6
9	Ag-Water	4%	200-1200	6
10	Cu-Water	1%	200-1200	6
11	Cu-Water	3%	200-1200	6
12	Cu-Water	4%	200-1200	6
13	Fe ₃ O ₄ -water	1%	200-1200	6
14	Fe ₃ O ₄ -water	3%	200-1200	6
15	Fe ₃ O ₄ -water	4%	200-1200	6
16	SiO ₂ -water	1%	200-1200	6
17	SiO ₂ -water	3%	200-1200	6
18	SiO ₂ -water	4%	200-1200	6
19	Ag,Cu,Fe ₃ O ₄ - ethyleneglycol(C ₂ H ₆ O ₂)	1%	200-1200	6
20	Ag,Cu,Fe ₃ O ₄ - ethyleneglycol(C ₂ H ₆ O ₂)	3%	200-1200	6

21	Ag,Cu,Fe ₃ O ₄ - ethyleneglycol(C ₂ H ₆ O ₂)	4%	200-1200	6
22	Al ₂ O ₃ ,TiO ₂ ,SiO ₂ - ethyleneglycol (C ₂ H ₆ O ₂)	1%	200-1200	6
23	Al ₂ O ₃ ,TiO ₂ ,SiO ₂ - ethyleneglycol (C ₂ H ₆ O ₂)	3%	200-1200	6
24	Al ₂ O ₃ ,TiO ₂ ,SiO ₂ - ethyleneglycol (C ₂ H ₆ O ₂)	4%	200-1200	6

5.1.6 Material Properties

The NIST is an institute that maintains very large information of material properties, including pure fluids and mixtures. The NIST database was utilized to obtain temperature-dependent properties of deionized water. REFPROP was developed by NIST and integrated into ANSYS Fluent, provides a comprehensive source of temperature-dependent fluid properties. REFPROP employs a combination of theoretical and predictive techniques for fluid property calculations.

For validation purposes De-ionized water is used a working fluid with temperature varying properties like viscosity (μ), specific heat (C_p), and thermal conductivity (k). Following properties were found in the material data sheet and are defined in ANSYS Fluent as shown in table 5.6.

Table 5.3: De-Ionized Water and Properties

Symbol	De-ionized water[[74],[75]]
μ (Pa.s)	$0.0194 - 1.065 \times 10^{-4}T + 1.489 \times 10^{-7}T^2$
k (W/m.k)	$-0.829 + 0.0079T - 1.04 \times 10^{-5}T^2$
C_p (J/kg.k)	$5348 - 7.42T + 1.17 \times 10^{-2}T^2$
ρ (kg/m ³)	998.2

To find material effective properties of nanoparticles with base fluids following correlations are used as described by Ahmed [69] for single nanofluid. The nanofluid was

integrated in the program as a homogenous fluid by specifying its effective properties. Equations 5.1, 5.2, 5.3, and 5.4 were utilized to compute the effective density (ρ_{eff}), specific heat capacity (C_{p_eff}), nanofluid viscosity (μ_{eff}), and thermal conductivity (k_{nf}) for different volume fractions (ϕ). In these equations, ρ_f denotes the base fluid's density.

Density:

$$\rho_{eff} = \phi\rho_p + (1 - \phi)\rho_f \dots\dots\dots 5.1$$

Specific heat:

$$C_{p_eff} = \frac{(1-\phi)(\rho C_p)_f + \phi(\rho C_p)_p}{(1-\phi)\rho_f + \phi\rho_p} \dots\dots\dots 5.2$$

Viscosity:

$$\mu_{eff} = \mu_f(1 + 39.11\phi + 533.9\phi^2) \dots\dots\dots 5.3$$

Thermal Conductivity:

$$\frac{k_{nf}}{k_f} = \frac{k_s + 2k_f - 2\delta(k_f - k_s)}{k_s + 2k_f + \delta(k_f - k_s)} \dots\dots\dots 5.4$$

For Trihybrid fluids following correlations are being used [76].

Density:

$$\rho_{thnf} = \phi_1 \rho_1 + (1 - \phi_1)\{(1 - \phi_2)[(1 - \phi_3)\rho_f + \phi_3\rho_3] + \phi_2\rho_2\} \dots\dots\dots 5.5$$

Viscosity:

$$\mu_{thnf} = \frac{\mu_f}{(1-\phi_1)^{2.5}(1-\phi_2)^{2.5}(1-\phi_3)^{2.5}} \dots\dots\dots 5.6$$

Specific heat:

$$C_{p_thnf} = \frac{(1-(\phi_1+\phi_2+\phi_3))((\rho C_p)_f + \phi_1(\rho C_p)_1 + \phi_2(\rho C_p)_2 + \phi_3(\rho C_p)_3)}{\rho_{thnf}} \dots\dots\dots 5.7$$

Thermal Conductivity:

$$\frac{k_{nf}}{k_f} = \frac{k_3 + 2k_f - 2\phi_3(k_f - k_3)}{k_3 + 2k_f + \phi_3(k_f - k_3)} \dots\dots\dots 5.8$$

$$\frac{k_{hnf}}{k_{nf}} = \frac{k_2 + 2k_{nf} - 2\phi_2(k_{nf} - k_2)}{k_2 + 2k_{nf} + \phi_2(k_{nf} - k_2)} \dots\dots\dots 5.9$$

$$\frac{k_{thnf}}{k_{hnf}} = \frac{k_1 + 2k_{hnf} - 2\phi_1(k_{hnf} - k_1)}{k_1 + 2k_{hnf} + \phi_1(k_{hnf} - k_1)} \dots\dots\dots 5.10$$

Here ρ_{thnf} is density, C_{p_thnf} is specific heat, μ_{thnf} represents viscosity and k_{thnf} is thermal conductivity of trihybrid nanofluid, while k_{hnf} is the thermal conductivity hybrid

Nano-fluid and similarly ϕ_1 , ϕ_2 , ϕ_3 are the volume fraction of the nanoparticles inside base fluid.

Table 5.4: Nanofluids Properties

Name	Concentration	ρ (kg/m ³)	C _p (J/kg.k)	μ (Pa.s)	k (W/m.k)
Al ₂ O ₃ -Water	1%	1027.72	4048.081287	0.002022286	0.624265086
Al ₂ O ₃ -Water	3%	1087.16	3805.881655	0.003715334	0.660432359
Al ₂ O ₃ -Water	4%	1116.88	3694.44918	0.004786096	0.67905516
CuO-Water	1%	1053.02	3955.875862	0.002022286	0.623492883
CuO-Water	3%	1163.06	3571.242412	0.003715334	0.658025748
CuO-Water	4%	1218.08	3404.986208	0.004786096	0.675783704
Ag-Water	1%	1093.02	3801.027063	0.002022286	0.625006286
Ag-Water	3%	1283.06	3211.475535	0.003715334	0.662746266
Ag-Water	4%	1378.08	2977.675026	0.004786096	0.682203345
Cu-Water	1%	1077.35	3865.332204	0.002022286	0.625000817
Cu-Water	3%	1236.05	3357.199911	0.003715334	0.662729179
Cu-Water	4%	1315.4	3149.112513	0.004786096	0.682180088
Fe ₃ O ₄ -water	1%	1039.82	4005.144737	0.002022286	0.621992923
Fe ₃ O ₄ -water	3%	1123.46	3694.487387	0.003715334	0.653362915
Fe ₃ O ₄ -water	4%	1165.28	3555.882191	0.004786096	0.669453502
SiO ₂ -water	1%	1010.02	4104.264866	0.002022286	0.611185483
SiO ₂ -water	3%	1034.06	3958.076707	0.003715334	0.620223103
SiO ₂ -water	4%	1046.08	3887.502294	0.004786096	0.624775571
Ag,Cu,Fe ₃ O ₄ - ethyleneglycol(C ₂ H ₆ O ₂)	1%	1326.738	2015.259696	0.019814678	0.271673
Ag,Cu,Fe ₃ O ₄ - ethyleneglycol(C ₂ H ₆ O ₂)	3%	1732.192	1559.690219	0.023092076	0.322376
Ag,Cu,Fe ₃ O ₄ - ethyleneglycol(C ₂ H ₆ O ₂)	4%	1927.602	1408.830242	0.0249584	0.350639
Al ₂ O ₃ ,TiO ₂ ,SiO ₂ - ethyleneglycol (C ₂ H ₆ O ₂)	1%	1190.441	2233.25258	0.019814678	0.268479
Al ₂ O ₃ ,TiO ₂ ,SiO ₂ - ethyleneglycol (C ₂ H ₆ O ₂)	3%	1334.485	1990.419185	0.023092076	0.311422
Al ₂ O ₃ ,TiO ₂ ,SiO ₂ - ethyleneglycol (C ₂ H ₆ O ₂)	4%	1404.706	1890.074222	0.0249584	0.335046

5.1.7 Boundary Condition

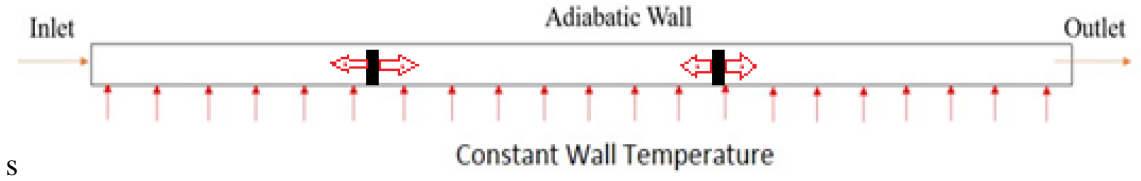


Figure 5.4 Boundary Conditions

A no-slip boundary condition was implemented at walls, yielding zero velocity components ($u = v = 0$). The velocity boundary condition at the intake was established according to the Reynolds number, which varied from 200 to 1200. The intake fluid temperature is set at 298 K. A pressure boundary condition was applied at the outlet, and the fluid dynamics were examined across different cross-sections and velocities. The base and LVG walls were kept at a constant temperature of 323.15 K, whereas the top and side walls of the single-channel arrangement were treated as adiabatic. The remaining side was designated as a symmetry border. It is essential to understand that velocity varies among different nanofluids at varying concentrations.

Inlet boundary:
$$u = v = 0, w = U_{in}, T = T_{in} = 298.15 (K)$$

Outlet boundary:
$$\frac{\partial u}{\partial z} = \frac{\partial v}{\partial z} = \frac{\partial w}{\partial z} = 0, \frac{\partial T}{\partial z} = 0$$

Symmetry Plane:
$$\frac{\partial v}{\partial x} = \frac{\partial w}{\partial x} = 0, \frac{\partial T}{\partial x} = \frac{\partial T_{sl}}{\partial x} = 0, u = 0$$

Heated wall:
$$u = v = w = 0, T = T_{wall} = 323.15(K)$$

Adiabatic walls:
$$u = v = w = 0, \frac{\partial T}{\partial y} = \frac{\partial T_{sl}}{\partial y} = 0$$

5.1.8 Solution methodology

Computational Fluid Dynamics (CFD) techniques provide powerful problem-solving tools. In this study, the experimental results of Liu et al. [43] (G2 configuration) were used to validate the simulation results and ensure the accuracy of the solution method. ANSYS Fluent was employed as the numerical computation platform for the microchannel heat exchanger models. The initial validation was conducted using deionized water as the working fluid. Subsequently, the material properties were modified according to Table 5.6 to explore the impact of different nanofluids. To simplify the simulation process, a single-phase flow model was adopted for the nanofluid. This approach is justified by the fact that the nanoparticles, due to their ultra-fine dimensions, are effectively suspended within the base fluid, leading to a uniform velocity and flow behavior between the particles and the fluid. The SIMPLE algorithm was utilized for velocity-pressure coupling, combined with second-order upwind. A convergence requirement of 0.00001 was instituted to ensure precise findings. The subsequent assumptions has been used for the heat transfer study within the microchannel:

1. Three-dimensional incompressible fluid having a steady-state formulation.
2. Temperature-dependent variable like specific heat, viscosity, and thermal conductivity and constant density were employed for deionized water (solely for validation purposes). Specific heat, viscosity and thermal conductivity are represented as piecewise linear functions of temperature, as demonstrated by Peiyi et al. and Okhotin et al. [[74],[75]].
3. Constant effective properties of the nanofluid are utilized.
4. Flow is presumed to be fully developed.
5. Radiation and viscous dissipation are disregarded.

Table 5.7 provides information about default under-relaxation factors used for numerical calculations.

Table 5.5 Relaxation factor

Factors	Value
Density	1.0
Momentum	0.7
Body Force	1.0
Pressure	0.3
Energy	1.0

By considering above assumptions, governing equations for description of fluid flow and heat transfer can be given as:

Mass continuity

$$\nabla(\rho\mathbf{V}) = 0 \quad 5.11$$

Momentum conservation

$$\mathbf{V} \cdot \nabla(\rho\mathbf{V}) = -\nabla p + \nabla \cdot (\mu \nabla \mathbf{V}) \quad 5.12$$

Energy conservation

$$\mathbf{V} \cdot \nabla(\rho C_p T_f) = \nabla \cdot (k_f \nabla T_f) \quad 5.13$$

Energy conservation

$$\nabla \cdot (k_w \nabla T_w) = 0 \quad 5.14$$

A uniform velocity boundary condition was applied at the inlet, while a pressure outlet boundary condition was imposed at the outlet due to the incompressible nature of the flow. No-slip boundary conditions were applied to the side walls, and an adiabatic boundary condition was assigned to the top wall. The bottom wall was maintained at a constant temperature.

5.2 Post Processing

This study focuses on the output parameters of Nusselt number, pressure drop, and friction factor. The pressure drop is directly derived from the simulation results, while the friction factor and Nusselt number are computed using proven relationships from the literature. The numerical simulation outcomes are delineated in relation to various

performance metrics. The Reynolds number (Re), a dimensionless metric that delineates the flow regime, is defined as follows:

$$Re = \frac{\rho_{eff} D_H v_{in}}{\mu_{eff}} \quad 5.15$$

Where

$$D_H = \frac{2wh}{(w + h)} \quad 5.16$$

Nusselt number (Nu) can be calculated by

$$Nu = \left(\frac{D_H}{k_{eff}} \right) \ln \left(\frac{(T_{wall} - T_i)}{(T_{wall} - T_o)} \right) \left(\frac{\dot{m} C_{p\,eff}}{A_{ht}} \right) \quad 5.17$$

Where, $C_{p\,eff}$ is specific heat, k_{eff} is thermal conductivity of fluid or nanofluid at mean temperature of fluid or nanofluid, T_s and T_i is bottom wall temperature and fluid inlet temperature respectively, \dot{m} is mass flow rate of fluid, T_o fluid outlet temperature and A_{ht} is area of base at which temperature is applied. Mean temperature can be calculated by equation

$$T_m = \frac{(T_i + T_o)}{2} \quad 5.18$$

The friction factor can be calculated by equation 5.19

$$f = \frac{D_H}{L} \frac{2\Delta P}{\rho_{eff} v_{in}^2} \quad 5.19$$

$$P_{power} = \Delta P \dot{V} \quad 5.10$$

Pumping power can be calculated by equation 5.20.

Where, \dot{V} is volume flow rate of fluid and ΔP is pressure difference is difference of pressure between outlet and inlet or in this case can be directly find out through fluent.

Poiseuille number equation is calculated by equation 5.21 [3]:

$$P_o = fRe \quad 5.11$$

Where value of P_o can be calculated from Shah and London [16] for micro-channel

$$P_o = 24(1 - 1.13553\alpha_{ch} + 1.9467\alpha_{ch}^2 - 1.7012\alpha_{ch}^3 + 0.9564\alpha_{ch}^4 - 0.2537\alpha_c^5) \quad 5.12$$

Heat transfer co-efficient (h) can be found by

$$h = \frac{Q}{A_{ht}\Delta T} \quad 5.13$$

Where

$$Q = \dot{m}C_{p\,eff}(T_o - T_i) \quad 5.14$$

In the above equation Q is total heat rate. There is quantity called thermal performance factor (TPF) shown in equation 5.25. This factor helps to select the best model out of all the investigated cases.

$$TPF = \frac{\left(\frac{Nu}{Nu_o}\right)}{\left(\frac{f}{f_o}\right)^{\frac{1}{3}}} \quad 5.15$$

In this equation Nu and f is the Nusselt number and friction factor of the studied model and Nu_o and f_o are the Nusselt number and friction factor of the reference model.

5.2.1 Grid Independence

A grid independence study was conducted using six different grid sizes on the G2 geometry of Chen et al[44] geometry and fluid deionized water at Reynolds numbers of 600: 128000 (Very Coarse), 170000 (Coarse), 216000 (Coarse), 320000 (Fine), 440000 (Fine), and 599120 (Very Fine). Table 4 presents the Nusselt number (Nu) results obtained for these grid sizes at a Reynolds number of 600. The analysis revealed no significant difference in the computed results between the very fine and extremely fine grids. To achieve a balance between accuracy, computational time, and costs, the very fine grid was selected for the subsequent simulations.

Table 5.6 Single Channel Mesh Characteristics

Number of elements	Nusselt Number	% Error
128000 (Very Coarse)	7.606	-
170000 (Coarse)	7.613	0.092
216000(Coarse)	7.615	0.023
320000 (Fine)	7.61533	0.00131
440000 (Fine)	7.61355	0.0233
599120(Very Fine)	7.61084	0.035

CHAPTER 6. RESULTS AND DISCUSSION

6.1 Data Validation

To validate the accuracy and reliability of the solver, the numerical results were compared against experimental data presented by Chen et al. [44] and by Hansel et al. [77] focusing on Nusselt Number and friction factor. The experimental setup in Chen et al. [44] consisted of a rectangular silicon microchannel with a hydraulic diameter of $160.5\ \mu\text{m}$ and a length of twenty millimeters, using deionized water as the coolant. The Reynolds number, based on the channel hydraulic diameter, varied from 200 to 1200. Computations were performed on a single symmetrical part of one configurations described in [44] which is a smooth channel. For further details regarding the test cases and experimental setup, please refer to [44]. The effects of variable thermos-physical properties on the results were considered.

Figure compares the predicted Nusselt number (Nu) values to the experimental results. The numerical results demonstrate excellent agreement with the experimental data reported by Chen et al. [44]. The maximum deviation between numerical and experimental results for the smooth microchannel is less than 11%. It is important to note that the average uncertainties associated with the experimental apparatuses in determining the Nusselt number for the smooth microchannel were reported to be 19.6% [44]. Additionally, a larger deviation was observed when using constant thermos-physical properties. , the selected model demonstrated reasonable agreement with the existing data for deionized water as the working fluid, with an average error of 3.5% for the Nusselt number (Nu) and 2.5% for the friction factor (f)

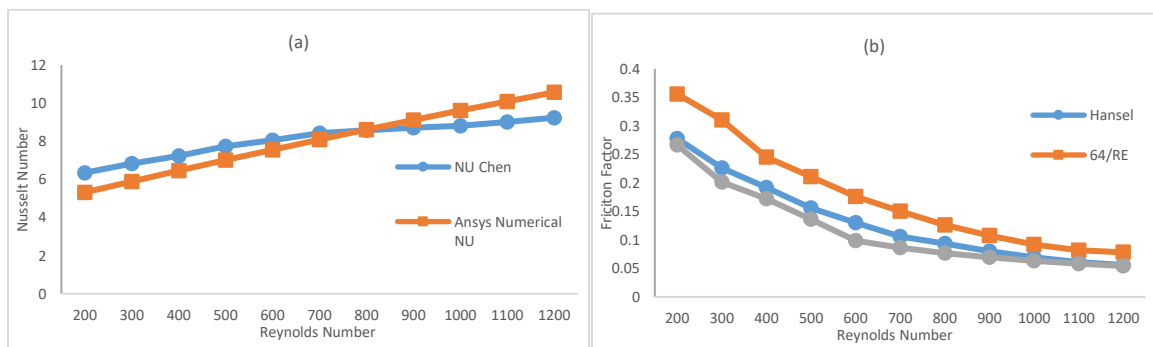


Figure 6.1: Data validation for (a) Nusselt Number (Chen. et al) and (b) friction factor (Hansel)

6.2 Effect of nanofluids on Nusselt Number

In this section following effects will be observed:

1. Several single and trihybrid nanoparticles effect on Nusselt number
2. Effect of concentration(1%,3% and 4%) of any single and trihybrid nanofluid on Nusselt number

6.2.1 Single and Tri-Hybrid nanofluids effect

The addition of nanoparticles to the base fluid can enhance both the viscosity and thermal conductivity of the overall fluid. Figure 6.2 illustrates the variation of Nusselt number against Reynolds number for 1%, 3% and 4% concentration of several nanofluids. For all nanofluids there is a significant improvement in Nusselt number. While a smooth transition in the trend is observed for several nanofluids with same concentration.

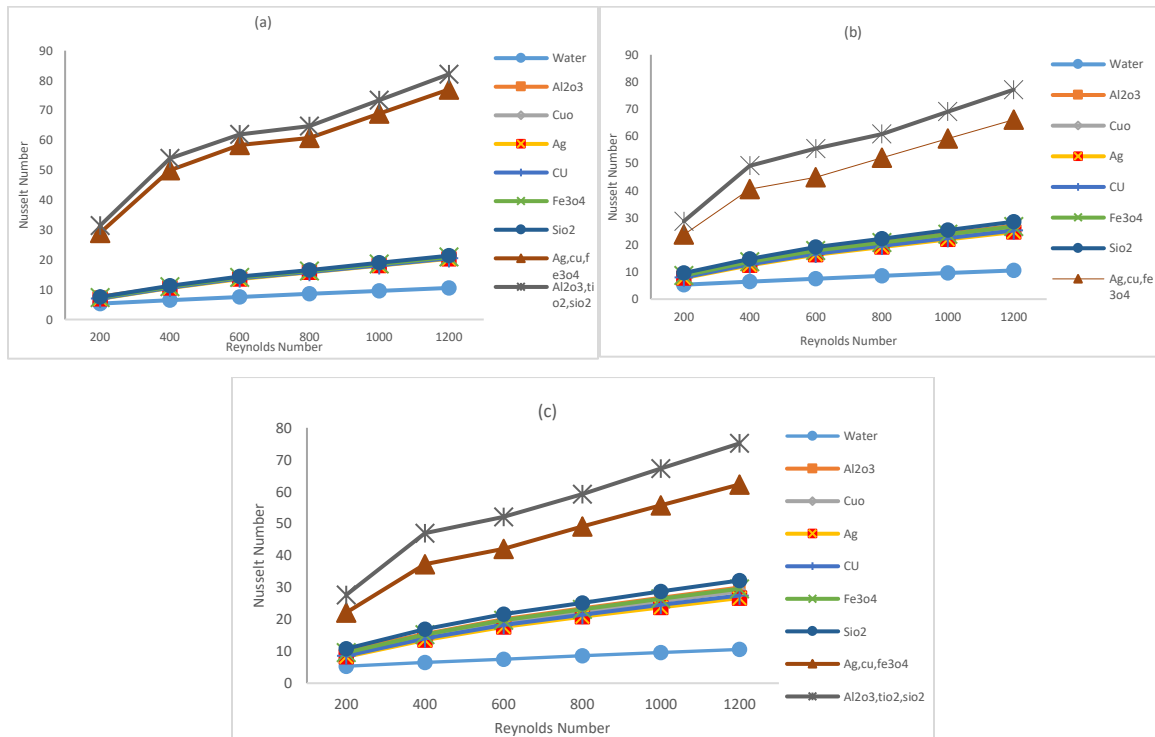


Figure 6.2: Nusselt number (Nu) comparison (a) 1% Nano-fluids (b) 3% Nano-fluids (c) 4% Nanofluids.

Compared to the base fluid without nanoparticles (0%) and without LVGs, the addition of 1%, 3%, and 4% nanoparticles loading results in an average improvement in convective heat transfer of 77%, 123%, and 145% for nanofluids containing single nanoparticles, respectively. Similarly, for trihybrid nanofluids a high increase of Nusselt

number is observed with average improvement of 631%, 541% and 501% observed with 1%, 3%, and 4% nanoparticle concentrations in base fluid of ethylene-glycol, respectively. The increase in thermal conductivity of the nanofluid is the primary factor contributing to the improved Nusselt number.

Here it can be seen that 1% nanoparticles loading shows the good Nusselt number results for trihybrid nanofluids but for single phase nanofluids higher concentration gives better results.

6.2.2 Effect of concentration of single & trihybrid nanofluids

Since the nanoparticle loading has effects on its thermos-physical properties hence figure 6.3 shows the effect of 1% , 2%, and 3% concentration of Al_2O_3 , CuO and SiO_2 nanofluids with in a microchannel having LVGs . It is evident from the figures that by increasing the concentration of nanoparticles in the base fluid Nusselt number increases. There is an average increase of 41%, 36% and 49% for Al_2O_3 , CuO and SiO_2 respectively.

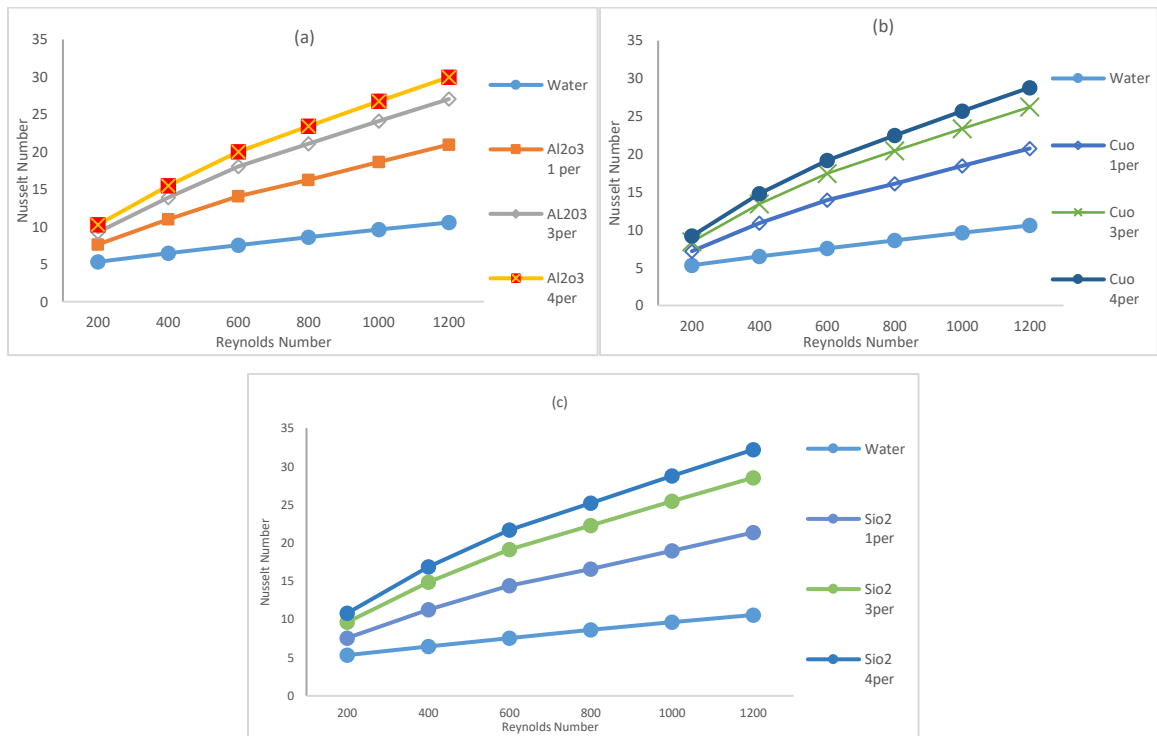


Figure 6.3: Nusselt number (Nu) comparison of 1%, 3%, 4% (a) Al_2O_3 (b) CuO (c) SiO_2

For tri-hybrid Nano-fluids this case is reversed, less the concentration of Nano-particle more will be the convective heat transfer. In figure 6.4 it is shown that average 29 % and 12% decrease of Nusselt is observed for $\text{AgCuFe}_3\text{O}_4$ and $\text{Al}_2\text{O}_3\text{SiO}_2\text{TiO}_2$ respectively.

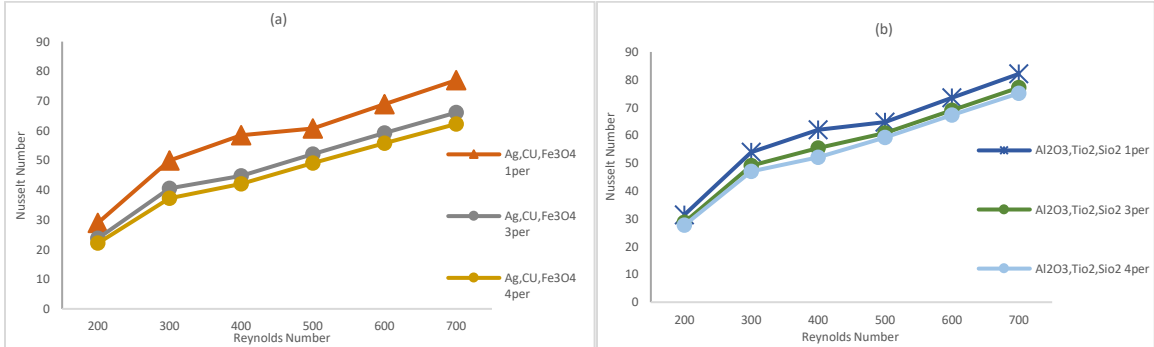


Figure 6.4: Nusselt number (Nu) comparison of 1%,3%,4% (a) $\text{AgCuFe}_3\text{O}_4$ (b) $\text{Al}_2\text{O}_3\text{SiO}_2\text{TiO}_2$

6.3 Effect of Nanofluids on apparent friction factor

To determine the pumping power needed to move the fluid inside the microchannel, the friction factor is necessary. In figure 6.5 it can be seen that many nanofluids with different concentration have same apparent friction factor value. As Reynolds number increases friction factor for all Nano fluids decreases due to the high velocities. As shown in figure 6.5 there is average of 24% decrease in friction factor at higher Reynolds number. Also same curve for all concentration because as the density increases for higher loadings of nanofluids so does the pressure drop.

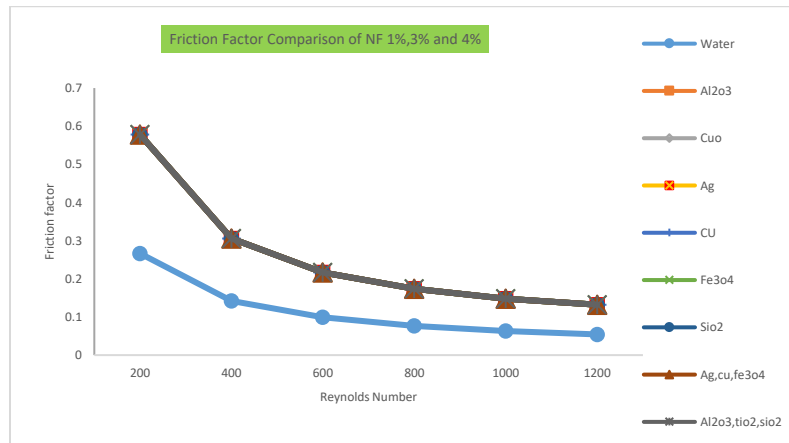


Figure 6.5: Friction factor data of single and tri-hybrid Nanofluids

6.4 Effect of Nanofluids on pressure

6.4.1 Effect of comparison of 1%, 3% and 4% nanofluids on change in pressure

In microchannel designing one main factor that need to be determined is change in pressure which tells that how much pumping power is required at the inlet for fluid to flow through the microchannel. In figures it can be seen that due to high viscosity and density a huge pumping power is required because of high pressure difference for trihybrid nanofluids as compared to the single nanofluids which require very less power. This shows that denser fluid require more pumping power.

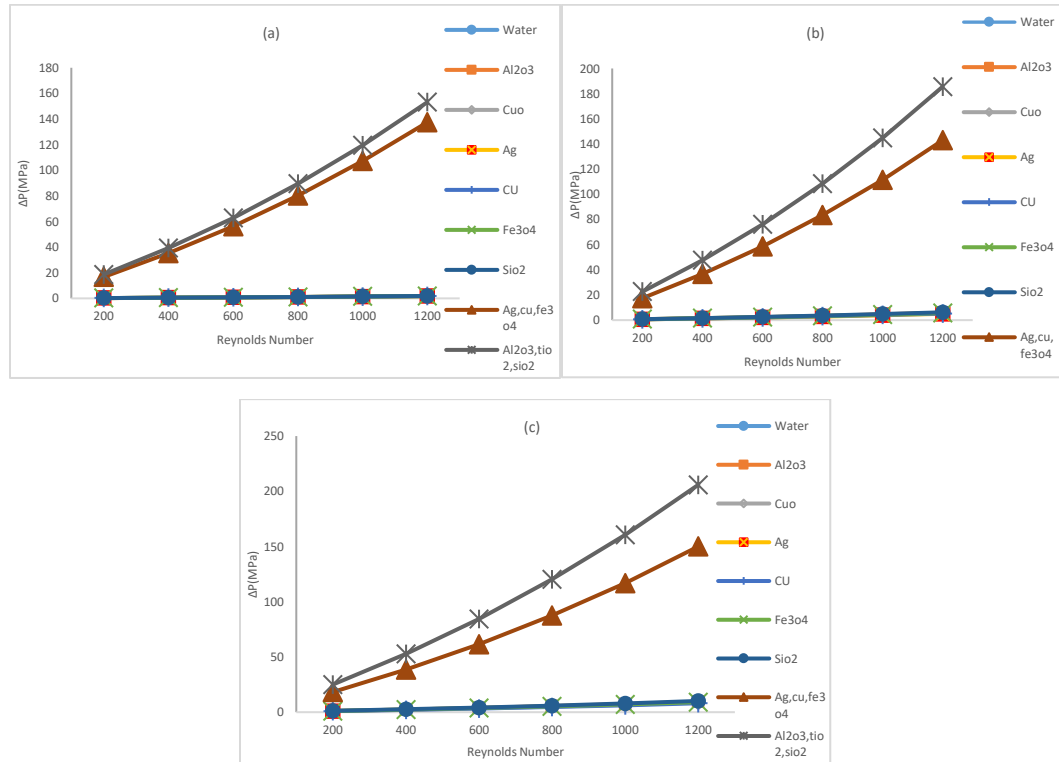


Figure 6.6: Pressure difference (a) 1% Nano-fluids (b) 3% Nano-fluids (c) 4% Nano-fluids

6.4.2 Effect of concentration nanofluids on change in pressure

Concentration effects the density and other material properties of the single and trihybrid nanofluids. Hence more the concentration higher will be the material properties of the nanofluid and higher pumping power will be then required. Following figure shows comparison between concertation of 1% 3% and 4% of Al_2O_3 and 1% 3% and 4% of $\text{Al}_2\text{O}_3\text{SiO}_2\text{TiO}_2$.The increment of pumping pressure among concentrations are in the order of hundreds

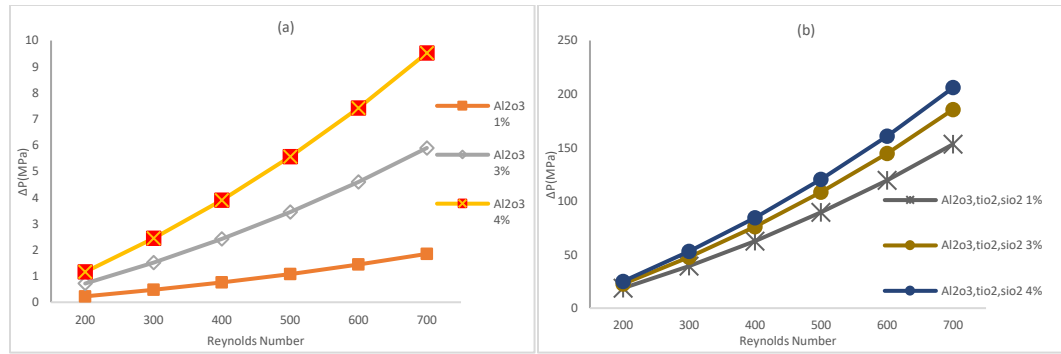


Figure 6.7: Pressure difference comparison of 1%, 3%, 4% (a) Al₂O₃ (b) Al₂O₃SiO₂TiO₂

Pressure changes around the LVGs and those contours can be seen in figure 6.8. At inlet and outlet there is low pressure as compared to around the LVGs. At 150° LVGs the pressure is higher at the inner side and at 30° LVGs higher pressure is along the walls.

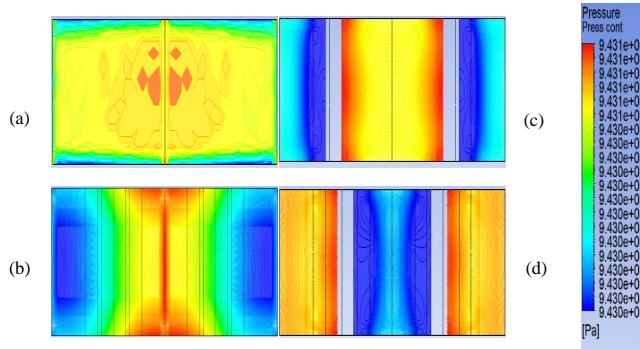


Figure 6.8: Pressure contour of 4% Al₂O₃SiO₂TiO₂ Re=1200 (a) Inlet (b) Outlet (c) 150° (d) 30°

6.5 Reynolds Number effect on base temperature

Reynolds numbers effect the heat carrying capacity of the fluid. In figure 6.9 there is comparison among Al₂O₃ 1% concentration at Reynolds number 1200 and Al₂O₃ of 1% concentration at Reynolds number 200 from inlet towards the outlet. Different temperature contours can be observed which depicts that same nanofluid at low Reynolds number take up more heat from the base while nanofluid at higher Reynolds doesn't get enough time to take heat from the bottom surface. The analysis of the Nusselt number indicates that at elevated temperatures, there is a reduction in convective heat transfer. This results in an increase in conductive heat transfer, which impairs the fluid's capacity to effectively transport heat. Increasing the flow rate can enhance the Nusselt number; however, this

typically results in a higher pressure drop, which is directly associated with the Reynolds number (Re).

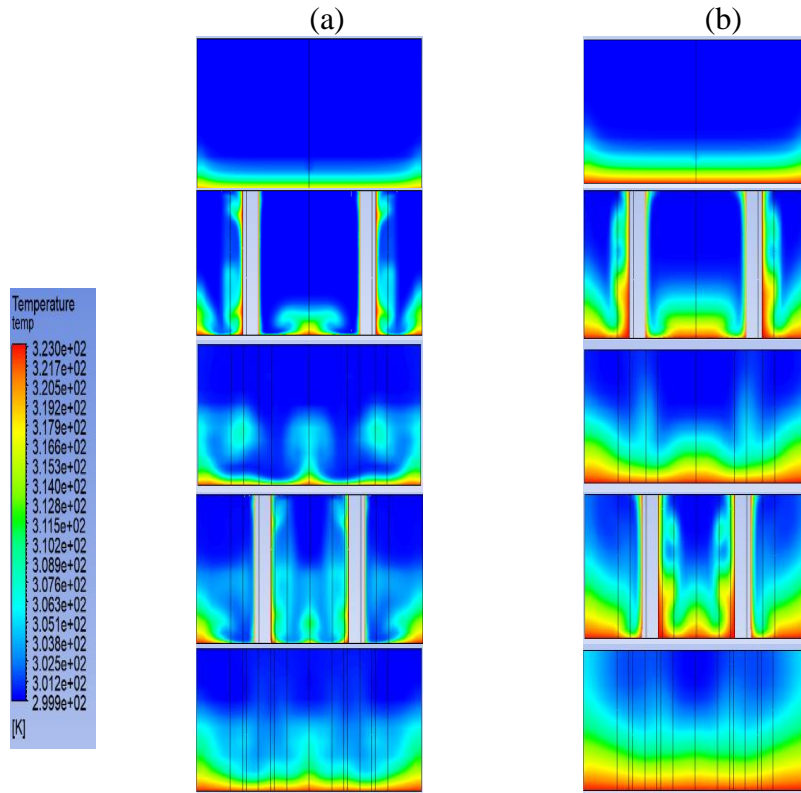


Figure 6.9: Temperature contours 1% Al₂O₃ inlet to outlet (upward to downwards) (a) Re=1200 (b) Re=200

The low-temperature region results from the rapid influx of fluid, which has insufficient time to transfer heat, whereas the high-temperature fluid zones arise from the reduced velocity of fluid during expansion after entering the plenum

Higher velocities along the length also increase the local Nusselt number due to vortex formation. These vortices are at RE=1200. Vortices allows the good mixing of cold and warm fluid which allows more convective heat transfer. Flow enter the channel and is developed before the LVGs. Flow behavior at LVGs is studied which involves generation of longitudinal vortices in micro-channel shown in Figure 6.10 for model having 100 micron width and height. Vortices promote convective heat transmission and aid in heat diffusion but also pressure drop increases. After LVGs flow start regaining fully developed form. The non-symmetric behavior of the velocity contours is caused by a rise in the kinetic

energy of fluid molecules, which results in an increase in the average speed of molecules, and since the channel is heated only from the bottom side, the behavior of the velocity contours develops accordingly.

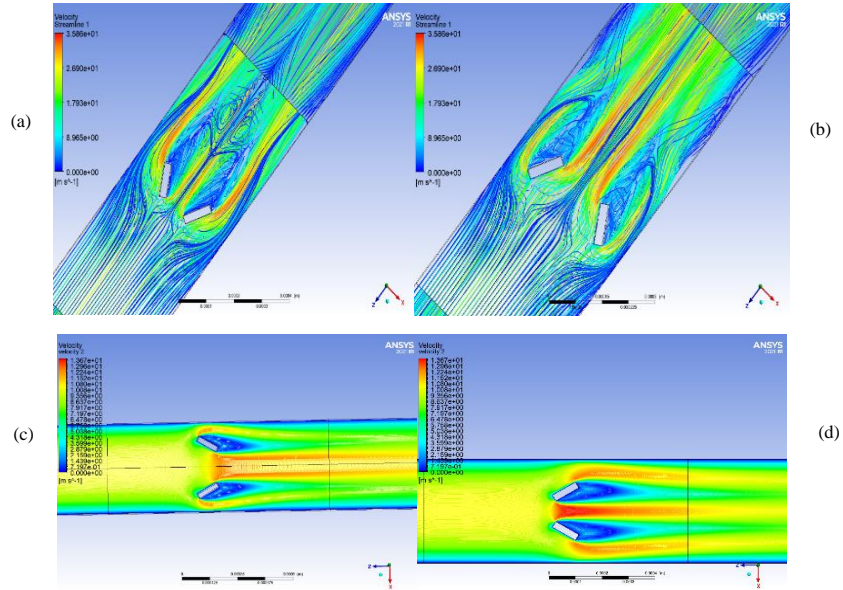


Figure 6.10: Velocity streamlines (a & b) and contours (c & d) around 150° and 30° LVGs

Furthermore, the flow disturbance generated by the LVGs are used to alleviate the flow separations in microchannel especially at high flow rate, thus improving heat transfer. It is have been noted that detailed design and geometrical location of LVGs within the microchannels can affect the properties of the vortices and downstream heat transfer as can be seen in figure above.

6.6 Effect of nanofluids on temperature

Nanofluids are very small particles but their addition in bas fluid can increase convective as well as conductive heat transfer. In section below following results are shown as an impact of Nano fluids on base and outlet temperature.

6.6.1 Effect on base temperature

Nanofluids are used with the concentration of 1%, 3% and 4% dispersed in water. Figure 6.11 shows comparison of Al_2O_3 nanofluid at different concentrations of 1%, 3% and 4% respectively. It can be seen that there is average of 2 to 3% change of temperature among concentrations. The nanofluid having low concentration have more temperature

locally than higher concentration nanofluids. This is due to the reason that low concentration nanofluids have low inlet velocity which allows that fluid to interact more with the heated surface

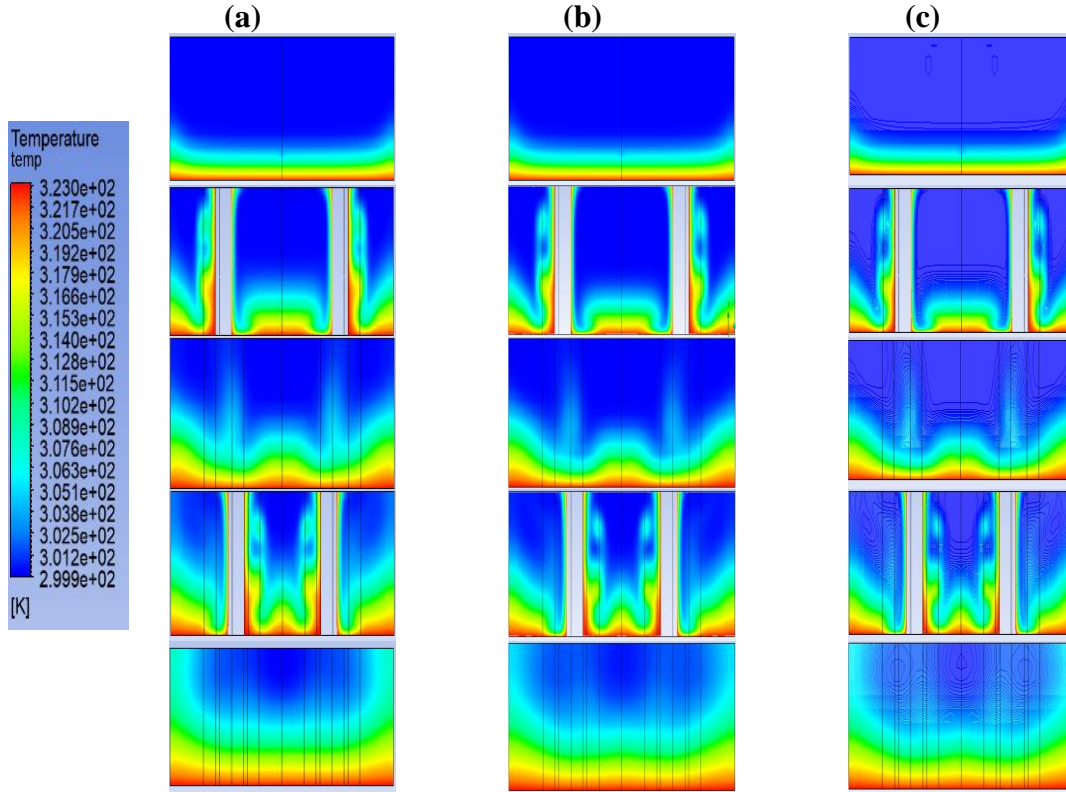


Figure 6.11: Temperature contours of Al_2O_3 at $Re=200$ at (a) 1% (b) 3% (c) 4%

6.6.2 Effect of concentration on Outlet temperature

It can be visualized through the graphical representation of 1%, 3% and 4% Al_2O_3 at varying Reynolds number that at lower Reynolds number and at lower concentrations the temperature of the fluid is more than at higher Reynolds number and higher concentrations. It can be seen that Al_2O_3 at 1 % and 200 Reynolds number have average temperature of 309K. But in the case of trihybrid nanofluids at more concentration fluids at low Reynolds number gives more outlet temperature.

The reason of higher outlet temperature by increasing particle loading in case trihybrid nanofluids is that thermal conductivity increases rapidly and we see conductive effect along with convective effect.

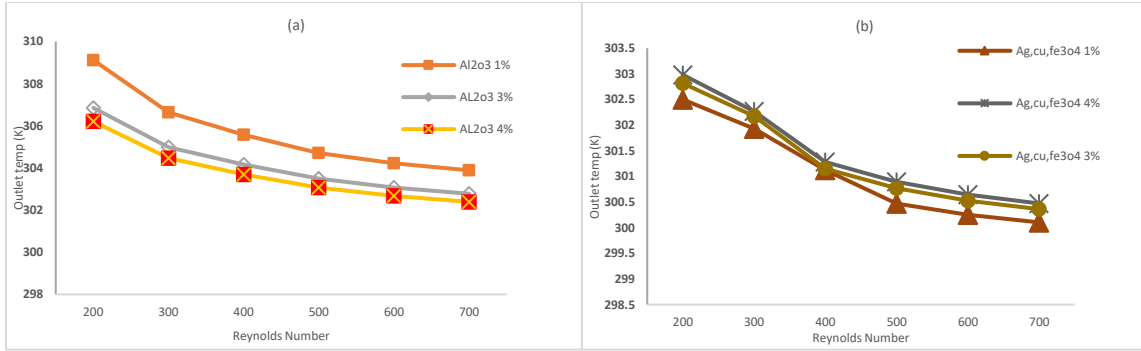


Figure 6.12: Outlet Temperature of 1%, 3%, 4% (a) Al₂O₃ and (b) AgCuFe₃O₄

LVGs cooling contours shown in Figure 6.12 provides information about physics of cooling in micro channel. Cooling at inlet is maximum which starts decreasing as fluid moves to the outlet of channel. While passing through the LVGs, fluid movement in laminar regime cause heat to diffuse hence, producing cooling and after it beside wall of channel. As, heat diffuses from center to outwards in chips to be cooled this cooling effect at LVGs is a suitable application.

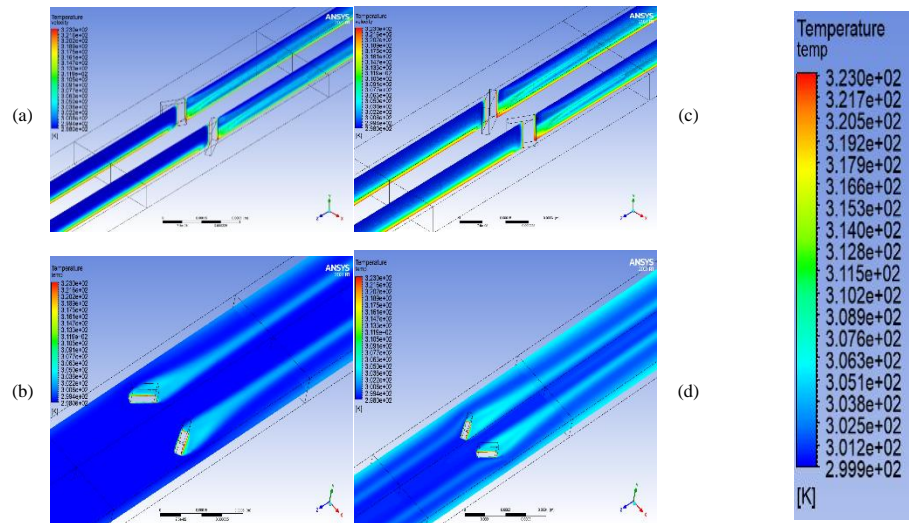


Figure 6.13: Temperature contours (a&b) 150°LVGs (c&d) 30°LVGs

LVGs having constant temperature boundary condition has highest temperature on its walls but as fluid passes through it heat is starting to be transmitted to the fluids around it. Nanofluid with low velocity and higher concentration takes good heat from LVGs boundaries but case is different for trihybrid fluids which acts oppositely.

6.6.3 Effect of nanofluids on Outlet temperature

Outlet temperature is a quantity which tells how much heat fluid is carrying within itself. Reynolds number and the concentration of the nanofluids has effect on outlet temperature too. Figure 6.13 shows that different nanofluids at same concentration have different outlet temperature this is because that their material properties varies among themselves and also due to concentrations. This graphs shows that among all the nanofluids under study Al_2O_3 with 1%, 3% and 4% concentration has the highest outlet temperature average of 307K at low Reynolds number but on the other hand it has very low Nusselt number at that point which can be explained due to its low specific heat constant.

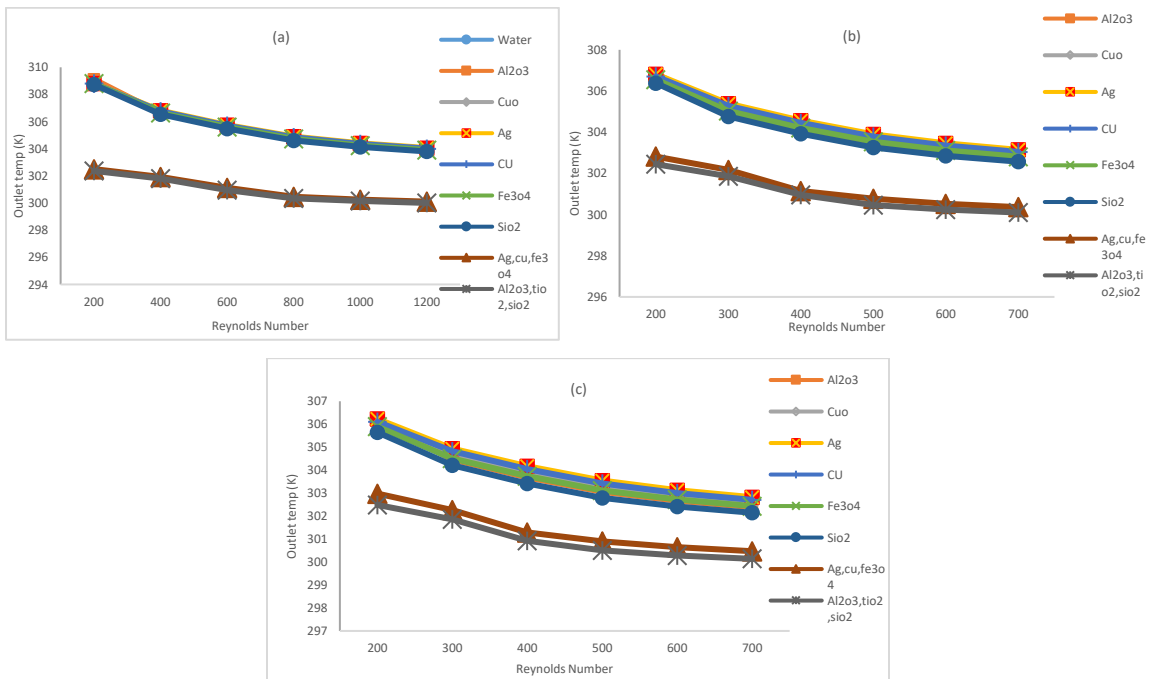


Figure 6.14: Outlet temperature of (a) 1% Nano-fluids (b) 3% Nano-fluids (c) 4% Nano-fluids

It can also be inferred from the figure 6.13 that even though trihybrid nanofluids have highest Nusselt number but their outlet temperature is very low suggesting that it only increases local Nusselt number. $Al_2O_3SiO_2TiO_2$ which have the highest Nusselt number has average outlet temperature of 300K.

Temperature of the fluid follows thermal boundary layer that temperature is maximum near the boundary and decreases with the fact that how much fluid particle is far

from heated surface. This same can be seen from the temperature contour of the microchannel at the bottom

LVGs are that why added to increases the fluid mixing for better heat transfer which can be visualized in the figure 6.14. LVGs allows the fluid in bottom layer to mix with upper layer fluid particles and consequently increase their temperature by effective heat transfer.

Following figure 6.14 shows the local temperature variation of the fluid along the length of the microchannel 5 micron above the base.

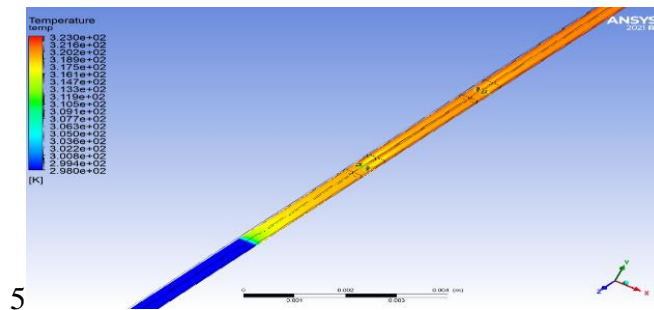


Figure 6.15: Temperature contour at bottom of microchannel

Figure 6.15 is shown here to understand temperature variation around LVGs and respective Nusselt number increase due to that first LVG that is at 0.005m and second LVG at 0.01m from the inlet we see a dip in temperature and then sudden temperature rise. That is the confirmation that LVGs are effective in increasing local temperature of the fluid by swirling the fluids with each other and letting it to transfer effective heat from heated surface to upper fluid layers.

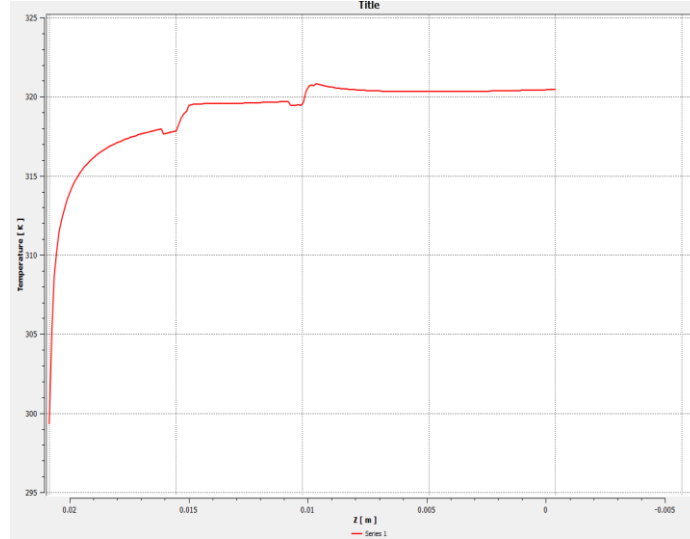


Figure 6.16: Temperature values of fluid at bottom of microchannel

The temperature while exiting the microchannel was increased to 323K at the bottom. This also show that nanoparticles plays effective role along with LVGs.

6.7 Effect of nanofluids on thermal performance factor (TPF)

Through study of flow and heat transfer behavior is made to find optimum model which could result in more heat transfer. The Thermal Performance Factor, is used to quantify the heat transfer capability by considering the relationship between the Nusselt number and friction factor. A TPF value greater than unity indicates that the analyzed model exhibits superior heat transfer performance compared to the reference model, while a decrease in TPF suggests a higher pressure drop. Figure illustrates the TPF values for different nanoparticle concentrations through LVGs equipped microchannels, using the 0% nanoparticle configuration (M4) [72] as the reference. For all models, among several single nanofluids of same concentration SiO₂ has the best performance while for trihybrid fluids Al₂O₃-TiO₂-SiO₂ in ethyleneglycol has highest TPF.

The average TPF values for single nanofluids with 1%, 3%, and 4% concentrations were 1.42, 1.78 and 1.97 respectively. Similarly, the average TPF values for trihybrid nanofluids with 1%, 3%, and 4% concentrations were 5.9, 5.2 and 4.95 respectively. It is evident from figure 6.16 that for single nanofluid increasing the particle loading increases its overall performance in the microchannel but for trihybrid nanofluids this effect is

opposite. The TPF of the Ag nanofluids were low through all Reynolds number for all concentrations, although the overall trend was similar.

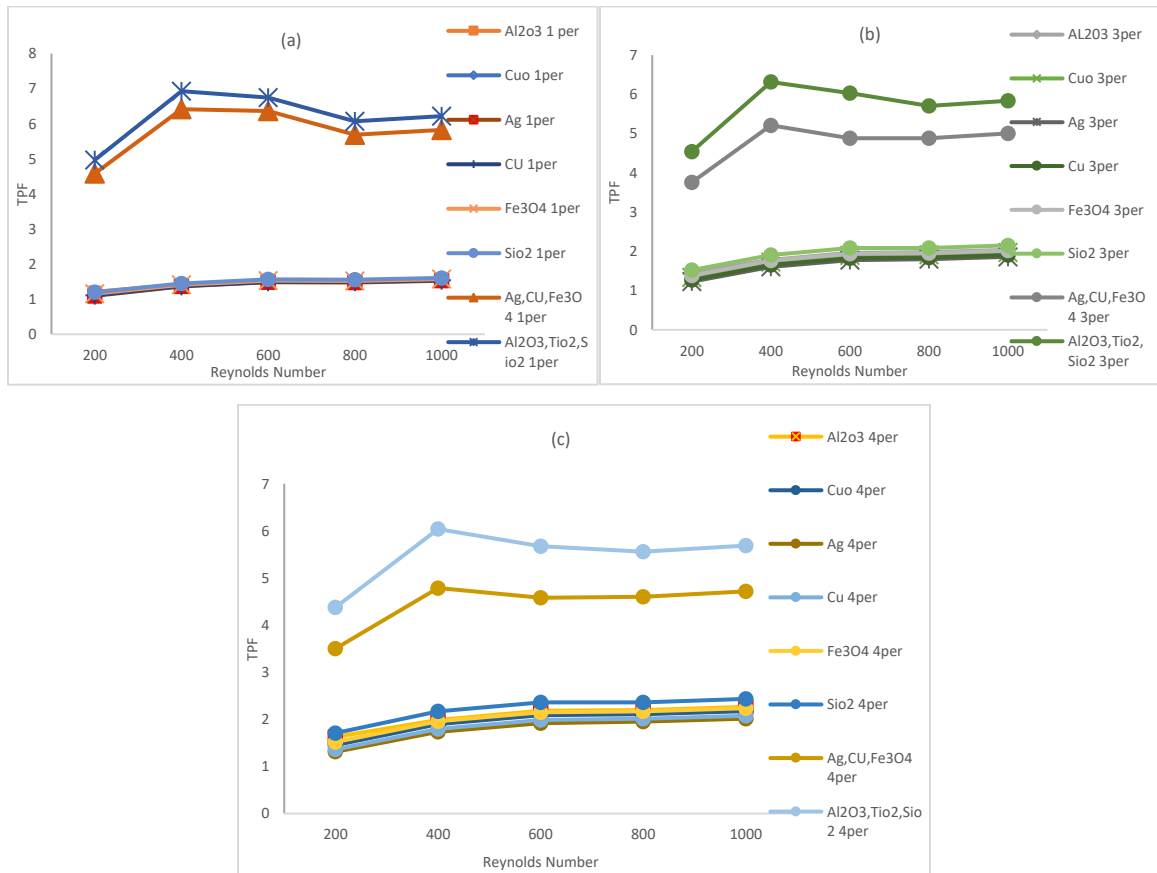


Figure 6.17: TPF of (a) 1% Nano-fluids (b) 3% Nano-fluids (c) 4% Nano-fluids

For some nanofluids of different concentrations it can be seen in Figure 6.17 that for trihybrid fluids increasing concentration decreases the TPF value. While for single phase nanofluids increasing concentration increases the TPF values.

Figure 6.18 provides all necessary information to select the most suitable model for micro-channel's Reynolds number and nanofluid along with their respective concentration.

Optimum performance point for a channel can be found as a trade-off between Nusselt number and friction factor Nusselt number.

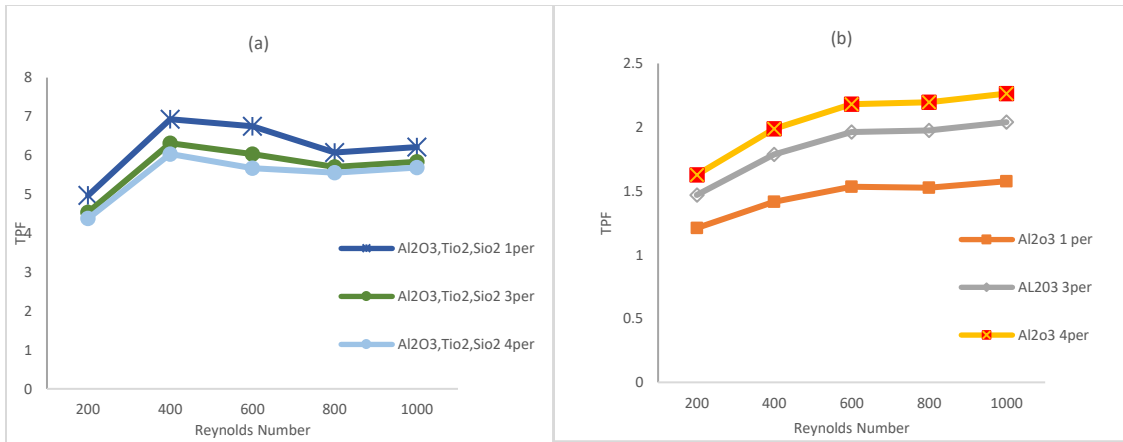


Figure 6.18: TPF of 1%, 3%, 4% (a) Al₂O₃SiO₂TiO₂ and (b) Al₂O₃

CHAPTER 7. CONCLUSION AND FUTURE RECOMMENDATION

The research quantitatively examined the impact of various nanoparticles and their concentrations within a microchannel integrated with LVGs on heat transfer efficiency under constant temperature boundary conditions. Al_2O_3 , TiO_2 , SiO_2 -ethylene glycol ($\text{C}_2\text{H}_6\text{O}_2$) Trihybrid nanofluids demonstrated the highest Nusselt number increase, exceeding 7.8% compared to the $\text{Ag,Cu,Fe}_3\text{O}_4$ -ethyleneglycol($\text{C}_2\text{H}_6\text{O}_2$) at the same nanoparticle concentration. Also around 10% as compared to the higher concentration of same trihybrid nanofluid. For all nanofluids with 1% nanoparticle addition, the Al_2O_3 , TiO_2 , SiO_2 -ethylene glycol ($\text{C}_2\text{H}_6\text{O}_2$) exhibited the greatest improvement of 583% compared to the 0% concentration of same microchannel with LVGs but at the cost of highest pumping pressure which may not be feasible. With 3% nanoparticle addition, all single and trihybrid nanofluids shows great improvement as compared to the 0% concentration channel. In terms of temperature reduction, the Al_2O_3 achieved a maximum average temperature drop of 14°C at $\text{Re} = 200$. The formation of vortices within the microchannel enhanced heat transfer by circulating heat from the base, thereby creating a cooling effect. Elevating the nanoparticle concentration resulted in an augmentation of both the Nusselt number and pressure drop; however, with trihybrid nanofluids, the opposite effect was observed. The development of regular counter-rotating vortices within channels contributed to reduced base temperatures. The construction of regular vortices at LVGs enhanced convective heat transfer and diminished pressure loss, whereas unpredictable flow patterns within the waves led to an increased pressure drop.

8. REFERENCES

- [1] D. Tuckerman and R. F. W. Pease, 'High-performance heat sinking for VLSI', *Electron Device Letters, IEEE*, vol. 2, pp. 126–129, Jun. 1981.
- [2] S. S. Mehendale, A. M. Jacobi, and R. K. Shah, 'Fluid Flow and Heat Transfer at Micro- and Meso-Scales With Application to Heat Exchanger Design', *Applied Mechanics Reviews*, vol. 53, no. 7, pp. 175–193, Jul. 2000.
- [3] S. Kandlikar, S. Garimella, D. Li, S. Colin, and M. R. King, *Heat Transfer and Fluid Flow in Minichannels and Microchannels*. Elsevier, 2005.
- [4] Obot, 'Toward a better understanding of friction and heat/mass transfer in microchannels - A literature review', *Microscale Thermophysical Engineering*, vol. 6, Nov. 2010.
- [5] T. Bayraktar and S. Pidugu, 'Characterization of liquid flow in microfluidic systems', *International Journal of Heat and Mass Transfer*, vol. 49, pp. 815–824, Mar. 2006.
- [6] M. Bahrami, M. Yovanovich, and J. Culham, 'Pressure Drop of Fully-Developed, Laminar Flow in Microchannels of Arbitrary Cross-Section', *Journal of Fluids Engineering-transactions of The Asme - J FLUID ENG*, vol. 128, Sep. 2006.
- [7] M. Bahrami, M. Yovanovich, and J. Culham, 'Pressure Drop of Fully Developed, Laminar Flow in Rough Microtubes', *Journal of Fluids Engineering-transactions of The Asme - J FLUID ENG*, vol. 128, May 2006.
- [8] X. F. Peng and B. X. Wang, 'Experimental investigation of heat transfer in flat plates with rectangular microchannels', *International Journal of Heat and Mass Transfer*, vol. 38, pp. 127–137, Jan. 1995.
- [9] A. Koyuncuoğlu, R. Jafari, T. Okutucu-Özyurt, and H. Külah, 'Heat transfer and pressure drop experiments on CMOS compatible microchannel heat sinks for monolithic chip cooling applications', *International Journal of Thermal Sciences*, vol. 56, pp. 77–85, 2012.
- [10] T. M. Harms, M. J. Kazmierczak, and F. M. Gerner, 'Developing convective heat transfer in deep rectangular microchannels', *International Journal of Heat and Fluid Flow*, vol. 20, no. 2, pp. 149–157, Apr. 1999.
- [11] Z. Li, W.-Q. Tao, and Y.-L. He, 'A numerical study of laminar convective heat transfer in microchannel with non-circular cross-section', *International journal of thermal sciences*, vol. 45, no. 12, pp. 1140–1148, 2006.
- [12] X. F. Peng, 'Convective heat transfer and flow friction for water flow in microchannel structures', *International Journal of Heat and Mass Transfer*, vol. 39, pp. 2599–2608, Jan. 1996.
- [13] W. Qu and I. Mudawar, 'Experimental and numerical study of pressure drop and heat transfer in a single-phase micro-channel heat sink', *International Journal of Heat and Mass Transfer*, vol. 45, no. 12, pp. 2549–2565, Jun. 2002.
- [14] Y. Mishan, A. Mosyak, E. Pogrebnyak, and G. Hetsroni, 'Effect of developing flow and thermal regime on momentum and heat transfer in micro-scale heat sink', *International Journal of Heat and Mass Transfer*, vol. 50, no. 15, pp. 3100–3114, Jul. 2007.
- [15] J. Lee and I. Mudawar, 'Assessment of the effectiveness of nanofluids for singlephase heat transfer in micro-channels', *International Journal of Heat and Mass Transfer*, vol. 50, pp. 452–463, Feb. 2007.

- [16] R. K. Shah and A. L. London, *Laminar Flow Forced Convection in Ducts: A Source Book for Compact Heat Exchanger Analytical Data*. Academic Press, 1978.
- [17] W. Qu and I. Mudawar, ‘Measurement and correlation of critical heat flux in two-phase micro-channel heat sinks’, *International Journal of Heat and Mass Transfer*, vol. 47, no. 10, pp. 2045–2059, May 2004.
- [18] A. Fedorov and R. Viskanta, ‘Three-dimensional conjugate heat transfer in the microchannel heat sink for electronic packaging’, *International Journal of Heat and Mass Transfer - INT J HEAT MASS TRANSFER*, vol. 43, pp. 399–415, Feb. 2000.
- [19] A. Mohamad Sahar, M. Ozdemir, and E. Fayyadh, ‘Single phase flow pressure drop and heat transfer in rectangular metallic microchannels’, *Applied Thermal Engineering*, vol. 93, pp. 1324–1336, Jan. 2016.
- [20] P.-S. Lee, S. V. Garimella, and D. Liu, ‘Investigation of heat transfer in rectangular microchannels’, *International Journal of Heat and Mass Transfer*, vol. 48, no. 9, pp. 1688–1704, Apr. 2005.
- [21] J.-T. Liu, X.-F. Peng, and W.-M. Yan, ‘Numerical study of fluid flow and heat transfer in microchannel cooling passages’, *International Journal of Heat and Mass Transfer*, vol. 50, no. 9, pp. 1855–1864, May 2007.
- [22] P. Rosa, T. Karayiannis, and M. Collins, ‘Single-phase heat transfer in microchannels: The importance of scaling effects’, *Applied Thermal Engineering*, vol. 29, pp. 3447–3468, Dec. 2009.
- [23] P. Hrnjak and X. Tu, ‘Single phase pressure drop in microchannels’, *International Journal of Heat and Fluid Flow*, vol. 28, pp. 2–14, Feb. 2007.
- [24] W. Bier, W. Keller, G. Linder, D. Seidel, K. Schubert, and H. Martin, ‘Gas to gas heat transfer in micro heat exchangers’, *Chemical Engineering and Processing: Process Intensification*, vol. 32, no. 1, pp. 33–43, 1993.
- [25] T. Stief, O.-U. Langer, and K. Schubert, ‘Numerical Investigations of Optimal Heat Conductivity in Micro Heat Exchangers’, *Chem. Eng. Technol.*, vol. 22, no. 4, pp. 297–303, Apr. 1999.
- [26] D. Liu and S. Garimella, ‘Investigation of Liquid Flow in Microchannels’, *Journal of Thermophysics and Heat Transfer - J THERMOPHYS HEAT TRANSFER*, vol. 18, pp. 65–72, Jan. 2004.
- [27] J. Xu, Y. Song, W. Zhang, H. Zhang, and Y. Gan, ‘Numerical simulations of interrupted and conventional microchannel heat sinks’, *International Journal of Heat and Mass Transfer*, vol. 51, no. 25–26, pp. 5906–5917, 2008.
- [28] G. Hetsroni, A. Mosyak, E. Pogrebnyak, and L. P. Yarin, ‘Fluid flow in microchannels’, *International Journal of Heat and Mass Transfer*, vol. 48, no. 10, pp. 1982–1998, 2005.
- [29] G. Hetsroni, A. Mosyak, E. Pogrebnyak, and L. P. Yarin, ‘Heat transfer in microchannels: Comparison of experiments with theory and numerical results’, *International Journal of Heat and Mass Transfer*, vol. 48, no. 25–26, pp. 5580–5601, 2005.
- [30] W. A. Phillips, *Experimental and numerical investigation of fluid flow and heat transfer in microchannels*. Louisiana State University and Agricultural & Mechanical College, 2008. Accessed: Oct. 19, 2024.
- [31] R. L. Webb and N. Y. Kim, ‘Enhanced heat transfer’, *Taylor and Francis, NY*, 2005, Accessed: Oct. 19, 2024.

- [32] A. M. Jacobi and R. K. Shah, 'Heat transfer surface enhancement through the use of longitudinal vortices: a review of recent progress', *Experimental Thermal and Fluid Science*, vol. 11, no. 3, pp. 295–309, 1995.
- [33] A. E. Bergles, 'Recent developments in enhanced heat transfer', *Heat and mass transfer*, vol. 47, no. 8, pp. 1001–1008, 2011.
- [34] T. R. Johnson and P. N. Joubert, 'The Influence of Vortex Generators on the Drag and Heat Transfer From a Circular Cylinder Normal to an Airstream', *Journal of Heat Transfer*, vol. 91, no. 1, pp. 91–99, Feb. 1969.
- [35] H. E. Ahmed, H. A. Mohammed, and M. Z. Yusoff, 'An overview on heat transfer augmentation using vortex generators and nanofluids: approaches and applications', *Renewable and Sustainable Energy Reviews*, vol. 16, no. 8, pp. 5951–5993, 2012.
- [36] A. Sohankar, 'Heat transfer augmentation in a rectangular channel with a vee-shaped vortex generator', *International journal of heat and fluid flow*, vol. 28, no. 2, pp. 306–317, 2007.
- [37] A. Sohankar Esfahani and L. Davidson, 'Numerical study of heat and fluid flow in a plate-fin heat exchanger with vortex generators', in *Turbulence Heat and Mass Transfer 4/Hanjalic, K., Nagano, Y., Tummers, MJ*, 2003, pp. 1155–1162.
- [38] L.-T. Tian, Y.-L. He, Y.-G. Lei, and W.-Q. Tao, 'Numerical study of fluid flow and heat transfer in a flat-plate channel with longitudinal vortex generators by applying field synergy principle analysis', *International Communications in Heat and Mass Transfer*, vol. 36, no. 2, pp. 111–120, 2009.
- [39] M. Fiebig, 'Embedded vortices in internal flow: heat transfer and pressure loss enhancement', *International Journal of Heat and Fluid Flow*, vol. 16, no. 5, pp. 376–388, 1995.
- [40] G. Biswas, H. Chattopadhyay, and A. Sinha, 'Augmentation of Heat Transfer by Creation of Streamwise Longitudinal Vortices Using Vortex Generators', *Heat Transfer Engineering*, vol. 33, pp. 406–424, Mar. 2012.
- [41] M. Fiebig, P. Kallweit, N. Mitra, and S. Tiggelbeck, 'Heat transfer enhancement and drag by longitudinal vortex generators in channel flow', *Experimental Thermal and Fluid Science*, vol. 4, no. 1, pp. 103–114, 1991.
- [42] J. M. Wu and W. Q. Tao, 'Effect of longitudinal vortex generator on heat transfer in rectangular channels', *Applied Thermal Engineering*, vol. 37, pp. 67–72, 2012.
- [43] C. Liu *et al.*, 'Experimental investigations on liquid flow and heat transfer in rectangular microchannel with longitudinal vortex generators', *International Journal of Heat and Mass Transfer*, vol. 54, no. 13–14, pp. 3069–3080, 2011.
- [44] C. Chen *et al.*, 'A study on fluid flow and heat transfer in rectangular microchannels with various longitudinal vortex generators', *International journal of heat and mass transfer*, vol. 69, pp. 203–214, 2014.
- [45] J. Lan, Y. Xie, and D. Zhang, 'Flow and heat transfer in microchannels with dimples and protrusions', 2012, Accessed: Oct. 19, 2024.
- [46] N. A. C. Sidik, M. N. A. W. Muhamad, W. M. A. A. Japar, and Z. A. Rasid, 'An overview of passive techniques for heat transfer augmentation in microchannel heat sink', *International Communications in Heat and Mass Transfer*, vol. 88, pp. 74–83, 2017.

- [47] A. Laitinen *et al.*, ‘A computational fluid dynamics study by conjugate heat transfer in OpenFOAM: A liquid cooling concept for high power electronics’, *International Journal of Heat and Fluid Flow*, vol. 85, p. 108654, 2020.
- [48] P. Bhuvankar and S. Dabiri, ‘Simulation of flow boiling in micro-channels: Effects of inlet flow rate and hot-spots’, *International Journal of Heat and Fluid Flow*, vol. 85, p. 108616, 2020.
- [49] M. N. Pantzali, A. G. Kanaris, K. D. Antoniadis, A. A. Mouza, and S. V. Paras, ‘Effect of nanofluids on the performance of a miniature plate heat exchanger with modulated surface’, *International Journal of Heat and Fluid Flow*, vol. 30, no. 4, pp. 691–699, 2009.
- [50] E. Ebrahimnia Bajestan, H. Niazmand, and M. Renksizbulut, ‘Flow and heat transfer of nanofluids with temperature dependent properties’, in *International Conference on Nanochannels, Microchannels, and Minichannels*, 2010, pp. 733–739.
- [51] W. Williams, J. Buongiorno, and L.-W. Hu, ‘Experimental Investigation of Turbulent Convective Heat Transfer and Pressure Loss of Alumina/Water and Zirconia/Water Nanoparticle Colloids (Nanofluids) in Horizontal Tubes’, *Journal of Heat Transfer-Transactions of The Asme - J HEAT TRANSFER*, vol. 130, Apr. 2008.
- [52] U. Rea, T. McKrell, L. Hu, and J. Buongiorno, ‘Laminar convective heat transfer and viscous pressure loss of alumina–water and zirconia–water nanofluids’, *International Journal of Heat and Mass Transfer*, vol. 52, no. 7–8, pp. 2042–2048, 2009.
- [53] Y. He, Y. Men, X. Liu, H. Lu, H. Chen, and Y. Ding, ‘Study on forced convective heat transfer of non-Newtonian nanofluids’, *Journal of Thermal Science*, vol. 18, pp. 20–26, 2009.
- [54] N. Akram *et al.*, ‘Experimental investigations of the performance of a flat-plate solar collector using carbon and metal oxides based nanofluids’, *Energy*, vol. 227, p. 120452, 2021.
- [55] K. Hosseinzadeh, A. Asadi, A. R. Mogharrebi, J. Khalesi, S. Mousavisani, and D. D. Ganji, ‘Entropy generation analysis of (CH₂OH)₂ containing CNTs nanofluid flow under effect of MHD and thermal radiation’, *Case Studies in Thermal Engineering*, vol. 14, p. 100482, 2019.
- [56] M. H. Fard, M. N. Esfahany, and M. R. Talaie, ‘Numerical study of convective heat transfer of nanofluids in a circular tube two-phase model versus single-phase model’, *International Communications in Heat and Mass Transfer*, vol. 37, no. 1, pp. 91–97, 2010.
- [57] Z. S. Kareem, H. H. Balla, and A. F. AbdulWahid, ‘Heat transfer enhancement in single circular impingement jet by CuO-water nanofluid’, *Case Studies in Thermal Engineering*, vol. 15, p. 100508, 2019.
- [58] R. S. Vajjha, D. K. Das, and P. K. Namburu, ‘Numerical study of fluid dynamic and heat transfer performance of Al₂O₃ and CuO nanofluids in the flat tubes of a radiator’, *International Journal of Heat and fluid flow*, vol. 31, no. 4, pp. 613–621, 2010.
- [59] H. M. Ammar *et al.*, ‘Heat transfer comparative analysis: straight channel and dimple-protrusion overlapping with copper oxide nano-particles’, in *2021 4th International Conference on Energy Conservation and Efficiency (ICECE)*, IEEE, 2021, pp. 1–8.
- [60] Y. He, Y. Men, Y. Zhao, H. Lu, and Y. Ding, ‘Numerical investigation into the convective heat transfer of TiO₂ nanofluids flowing through a straight tube under the

- laminar flow conditions’, *Applied Thermal Engineering*, vol. 29, no. 10, pp. 1965–1972, 2009.
- [61] W. H. Azmi, K. A. Hamid, A. I. Ramadhan, and A. I. M. Shaiful, ‘Thermal hydraulic performance for hybrid composition ratio of TiO₂–SiO₂ nanofluids in a tube with wire coil inserts’, *Case Studies in Thermal Engineering*, vol. 25, p. 100899, 2021.
- [62] A. K. Santra, S. Sen, and N. Chakraborty, ‘Study of heat transfer due to laminar flow of copper–water nanofluid through two isothermally heated parallel plates’, *International Journal of Thermal Sciences*, vol. 48, no. 2, pp. 391–400, Feb. 2009.
- [63] D. Xu, Y. Hu, and D. Li, ‘A lattice Boltzmann investigation of two-phase natural convection of Cu-water nanofluid in a square cavity’, *Case Studies in Thermal Engineering*, vol. 13, p. 100358, Mar. 2019.
- [64] F. Ahmed, ‘Experimental investigation of Al₂O₃-water nanofluid as a secondary fluid in a refrigeration system’, *Case Studies in Thermal Engineering*, vol. 26, p. 101024, Aug. 2021.
- [65] D. SÁCHICA, C. Treviño, and L. Martínez-Suástegui, ‘Numerical study of magnetohydrodynamic mixed convection and entropy generation of Al₂O₃ -water nanofluid in a channel with two facing cavities with discrete heating’, *International Journal of Heat and Fluid Flow*, vol. 86, p. 108713, Sep. 2020.
- [66] A. Behzadmehr, M. Saffar-Avval, and N. Galanis, ‘Prediction of turbulent forced convection of a nanofluid in a tube with uniform heat flux using a two phase approach’, *International Journal of Heat and Fluid Flow*, vol. 28, no. 2, pp. 211–219, Apr. 2007.
- [67] V. Bianco, F. Chiacchio, O. Manca, and S. Nardini, ‘Numerical investigation of nanofluids forced convection in circular tubes’, *Applied Thermal Engineering*, vol. 29, pp. 3632–3642, Jun. 2009.
- [68] V. Bianco, O. Manca, and S. Nardini, ‘Numerical investigation on nanofluids turbulent convection heat transfer inside a circular tube’, *International Journal of Thermal Sciences*, vol. 50, pp. 341–349, Mar. 2011.
- [69] H. E. Ahmed, H. A. Mohammed, and M. Z. Yusoff, ‘Heat transfer enhancement of laminar nanofluids flow in a triangular duct using vortex generator’, *Superlattices and Microstructures*, vol. 52, no. 3, pp. 398–415, Sep. 2012.
- [70] J. Lienhard, ‘A Heat Transfer Textbook’, *J Heat Transfer*, vol. 108, Jan. 2013.
- [71] S. Balaji and S. Lakshminarayanan, ‘Improved Design of Microchannel Plate Geometry for Uniform Flow Distribution’, *Can. J. Chem. Eng.*, vol. 84, no. 6, pp. 715–721, May 2008.
- [72] A. Ebrahimi, E. Roohi, and S. Kheradmand, ‘Numerical study of liquid flow and heat transfer in rectangular microchannel with longitudinal vortex generators’, *Applied Thermal Engineering*, vol. 78, pp. 576–583, Mar. 2015, doi: 10.1016/j.applthermaleng.2014.12.006.
- [73] D. Ting, *Thermofluids: From Nature to Engineering*. Elsevier Science, 2022.
- [74] W. Peiyi and W. A. Little, ‘Measurement of friction factors for the flow of gases in very fine channels used for microminiature Joule-Thomson refrigerators’, *Cryogenics*, vol. 23, no. 5, pp. 273–277, 1983.
- [75] A. Okhotin, A. Pushkarskii, and V. Gorbachev, ‘Thermophysical Properties of Semiconductors, Atom Publ’, *House, Moscow*, 1972.

- [76] W. Shinwari, T. Hayat, Z. Abbas, and S. Momani, 'Numerical study for trihybrid nanomaterial flow by convectively heated curved sheet', *Case Studies in Thermal Engineering*, vol. 53, p. 103962, Jan. 2024.
- [77] C. Hansel, 'Mapping of pressure losses through microchannels with sweeping-bends of various angle and radii', 2008